NAVAL POSTGRADUATE SCHOOL
Monterey, California

THESIS

OCEAN RESPONSE TO HURRICANE FORCING

by

Charles K. Hopkins

June 1982

Thesis Advisor: R. L. Elsberry

Approved for public release; distribution unlimited

SECURITY CLASSIFICATION OF THIS PAGE (When Data Entered)

REPORT DOCUMENTATION PAGE

READ INSTRUCTIONS BEFORE COMPLETING FORM

1. REPORT NUMBER

2. GOVT ACCESSION NO.

3. RECIPIENT'S CATALOG NUMBER

4. TITLE (and Subtitle)
Ocean Response to Hurricane Forcing

5. TYPE OF REPORT & PERIOD COVERED
Master's Thesis
June 1982

6. PERFORMING ORG. REPORT NUMBER

7. AUTHOR(s)
Charles K. Hopkins

8. CONTRACT OR GRANT NUMBER(s)

9. PERFORMING ORGANIZATION NAME AND ADDRESS
Naval Postgraduate School
Monterey, California 93940

10. PROGRAM ELEMENT, PROJECT, TASK AREA & WORK UNIT NUMBERS

11. CONTROLLING OFFICE NAME AND ADDRESS
Naval Postgraduate School
Monterey, California 93940

12. REPORT DATE
June 1982

13. NUMBER OF PAGES
89

14. MONITORING AGENCY NAME & ADDRESS(if different from Controlling Office)

15. SECURITY CLASS. (of this report)

15a. DECLASSIFICATION/DOWNGRADING SCHEDULE

16. DISTRIBUTION STATEMENT (of this Report)
Approved for public release; distribution unlimited

17. DISTRIBUTION STATEMENT (of the abstract entered in Block 20, if different from Report)

18. SUPPLEMENTARY NOTES

19. KEY WORDS (Continue on reverse side if necessary and identify by block number)
Hurricane ocean interaction, ocean buoy current measurements, ocean current prediction model, hurricane Frederic, ocean inertial-gravity waves, Gulf of Mexico, near-inertial internal waves, current meter data.

20. ABSTRACT (Continue on reverse side if necessary and identify by block number)
The current meter records collected at three sites in the Gulf of Mexico during the passage of Hurricane Frederic are analyzed to determine the storm-induced flow at various ocean depths, determine the associated energy increase and decay, and compare these observations to similar results from a numerical model. The records at the two deeper sites

DD FORM 1 JAN 73 1473 EDITION OF 1 NOV 65 IS OBSOLETE
S/N 0102-014-6601

SECURITY CLASSIFICATION OF THIS PAGE (When Data Entered)

(Block 20 continued)

are rather unique because they are within 100 km of the hurricane track. Pre-storm conditions are controlled by topography, and as the storm passes there is an abrupt change in the direction of flow and initiation of a strong inertial response at all levels of the two deeper sites. After this initial surge, the residual flow tends toward the pre-storm direction. The horizontal kinetic energy associated with inertial motion is calculated. The energy increase and decay is shown to vary with depth.

An embedded mixed-layer ocean circulation model (Adamec et al, 1981) is forced with an idealized storm translating at the same speed ($7.5 m\ s^{-1}$) as Frederic. The abrupt response and strong inertial component predicted by the model is qualitatively similar to the observations.

Approved for public release; distribution unlimited

Ocean Response to Hurricane Forcing

by

Charles K. Hopkins
Lieutenant, United States Navy
B.S. (Physical Oceanography), University of Washington, 1976
B.S. (Atmospheric Sciences), University of Wasington, 1976

Submitted in partial fulfillment of the
requirements for the degree of

MASTER OF SCIENCE IN METEOROLOGY AND OCEANOGRAPHY

from the

NAVAL POSTGRADUATE SCHOOL
June 1982

ABSTRACT

The current meter records collected at three sites in the Gulf of Mexico during the passage of Hurricane Frederic are analyzed to determine the storm-induced flow at various ocean depths, determine the associated energy increase and decay, and compare these observations to similar results from a numerical model. The records at the two deeper sites are rather unique because they are within 100 km of the hurricane track. Pre-storm conditions are controlled by topography, and as the storm passes there is an abrupt change in the direction of flow and initiation of a strong inertial response at all levels of the two deeper sites. After this initial surge, the residual flow tends toward the pre-storm direction. The horizontal kinetic energy associated with inertial motion is calculated. The energy increase and decay is shown to vary with depth.

An embedded mixed-layer ocean circulation model (Adamec et al, 1981) is forced with an idealized storm translating at the same speed (7.5m s^{-1}) as Frederic. The abrupt response and strong inertial component predicted by the model is qualitatively similar to the observations.

TABLE OF CONTENTS

LIST OF FIGURES

LIST OF TABLES

ACKNOWLEDGEMENT

Before all else, I would like to thank my advisor Russ Elsberry. His recognition of the importance of the data we used, extensive knowledge of the subject material, intelligence, attention to detail and patience have made this thesis enjoyable and challenging. I can not imagine having made a better choice of advisors. The efforts of Lynn K. Shay in obtaining the data for this thesis were noteworthy and greatly appreciated. This thesis would not have even been started were it not for his efforts. The majority of this thesis was performed using the facilities of the W. R. Church computer center. The computer center advisors, especially Dennis Mar, have been extremely helpful in providing solutions to programming problems. I would also like to thank the courteous, industrious computer operators for providing an invaluable service. Also, Dave Adamec willingly provided his time and efforts in modifying the model used in this thesis. Thankfully, my efforts in this area were minimal as a result. Dr. Dale Leipper provided the benefit of his knowledge and insight, giving this thesis direction from the beginning. I also would very much like to thank Bill Garwood for his review of this thesis from the oceanographic point of view.

I. INTRODUCTION

Several studies of the response of the ocean to hurricane passage have been made by such authors as Fisher (1958), Leipper (1967), Wright (1969), Pudov et al (1979) and Fedorov et al (1979). A review of the hydrographic, i.e. sea-surface temperature (SST), salinity temperature depth (STD), and expendable bathythermograph (XBT), surveys of several of these authors is given in Table I from Price (1981). The majority of these observations concentrate on the asymmetrical SST response, and the expected ocean mixed-layer response to hurricane passage of vertical mixing as the hurricane approaches, followed by upwelling in the wake of the storm (see e.g. Leipper, 1967; Friese, 1977). Additionally, oscillations on the order of the local inertial period have been noted in the temperature and current fields in the wake of open-ocean storms. The inertial response becomes complicated in the shoal waters of continental shelves and the ability to detect inertial motion is severely restricted (Mayer et al, 1981). The hurricane-induced upwelling decreases the mixed layer depth. The depth reaches a local minimum about one half inertial period after eye passage and continues to oscillate at about

the local inertial period for some period after the storm passage. Geisler (1970) presented the relationship between hurricane translation speed and the oscillatory response of the thermocline. If the hurricane translation speed is greater than the internal phase speed, typically about 2 m s^{-1}, and if its horizontal scale is comparable to the internal Rossby radius, currents throughout the affected area are controlled by a balance between the centrifugal and Coriolis accelerations.

TABLE I

Hydrographic Studies of the Sea Surface Temperature Response to Hurricanes (Price, 1981).

Study: Hurricane	Method: Region	Average U_H (m s^{-1})	Hurricane central pressure (mb)	ΔSST_{max} (°C)	Position of* ΔSST_{max}
Leipper (1967): Hilda (1964)	extensive post-hurricane hydrographic survey: Gulf of Mexico	3	930	−6	pattern is generally unclear, may be 50 km to left of track (Fig. 8)
Fedorov *et al.* (1979): Ella (1968)	Extensive pre- and post-hurricane XBT survey: mid-Atlantic	6	980	−2	30 km to right (Fig. 3, same as this Fig. 1a)
Pudov *et al.* (1979): Tess (1975)	extensive post-hurricane STD survey: mid-Pacific	6	940	−4	75 km to right (Fig. 1, same as this Fig. 2a)
Wright (1969): Shirley (1965)	1 pre-, 1 post-hurricane XBT section: vicinity of the Kuroshio	13	935	−3	20 km to right (Fig. 4)
Jordan (1964): Wanda (1956) Clara (1955)	extensive pre- and post-hurricane SST reports from ships of opportunity: mid-Pacific	16 18	920 915	−2 −1	150 km to right 50 km to right (Figs. 2 and 3)

*Estimates made by Price (1981) from their figures noted

The response to Hurricane Eloise as her eye passed over the National Oceanic and Atmospheric Administration's Data

Buoy Office (NDBO) EB-10 buoy has been studied extensively (see e.g. Martin, 1982; Price, 1981; Black and Withee, 1976). EB-10 was located in the central Gulf of Mexico and collected the first open-ocean data under a hurricane as reported by Withee and Johnson (1976). Mayer et al (1981) reported a study of the passage of Hurricane Belle over the continental shelf of the New York Bight on 10 August 1976. These continental shelf responses differ from the open-ocean responses due to the topographic influences of the shelf and large gradients in the physical properties between the shelf water and the deep ocean water.

Hurricane Frederic passed through the Gulf of Mexico between 11 and 13 September, 1979. The satellite data depicted in Figs. 1, 2, and 3 together with whatever XBT data collected during hurricane passage are usually the only type of data available to study these geophysically, socially and economically important events. However, during this period the Naval Oceanographic Office (NAVOCEANO), NSTL Station, Bay St. Louis, Mississippi operated three data buoys which collected a unique set of ocean temperature and current data. This thesis studies the ocean current response to the passage of Hurricane Frederic as it passed

near the three data buoys. Additionally a comparison of the real data to the results provided by the three-dimensional ocean model of Adamec et al (1981) is made. The hurricane forcing of the model is idealized rather than being formulated to represent the actual hurricane, but a translation speed of 7.5 m s^{-1}, the same as for Frederic, is used.

The buoy current data provided by NAVOCEANO indicate that the flow associated with the passage of Hurricane Frederic had a large inertial component after the storm passed. The rate at which the inertial flow damps, and the rate at which it propagates with depth, are determined from the buoy data and compared to the model.

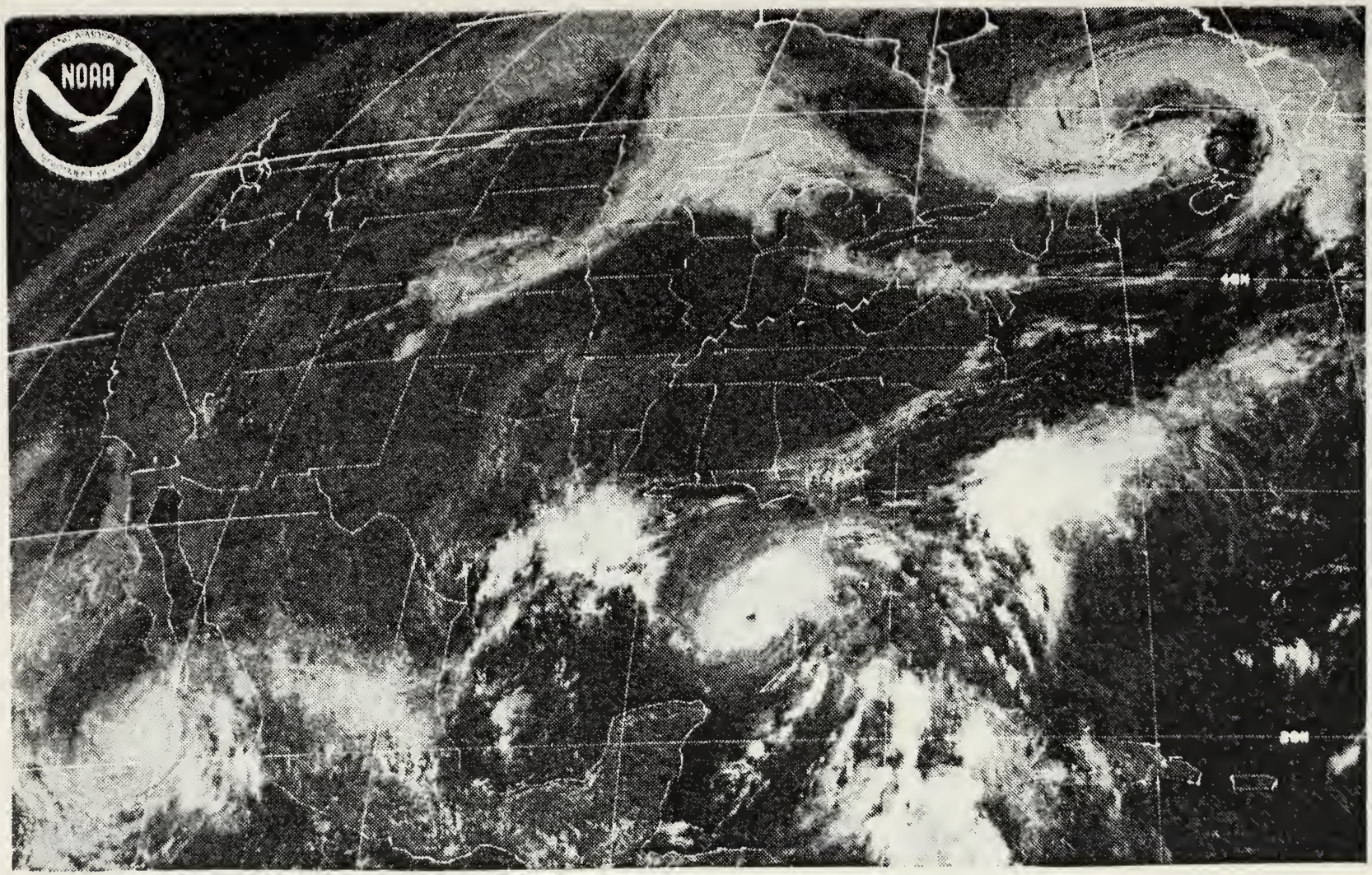

Figure 1. U.S. cloud cover, 1700 GMT 11 September 1979, NOAA satellite photograph, National Environment Satellite Service.

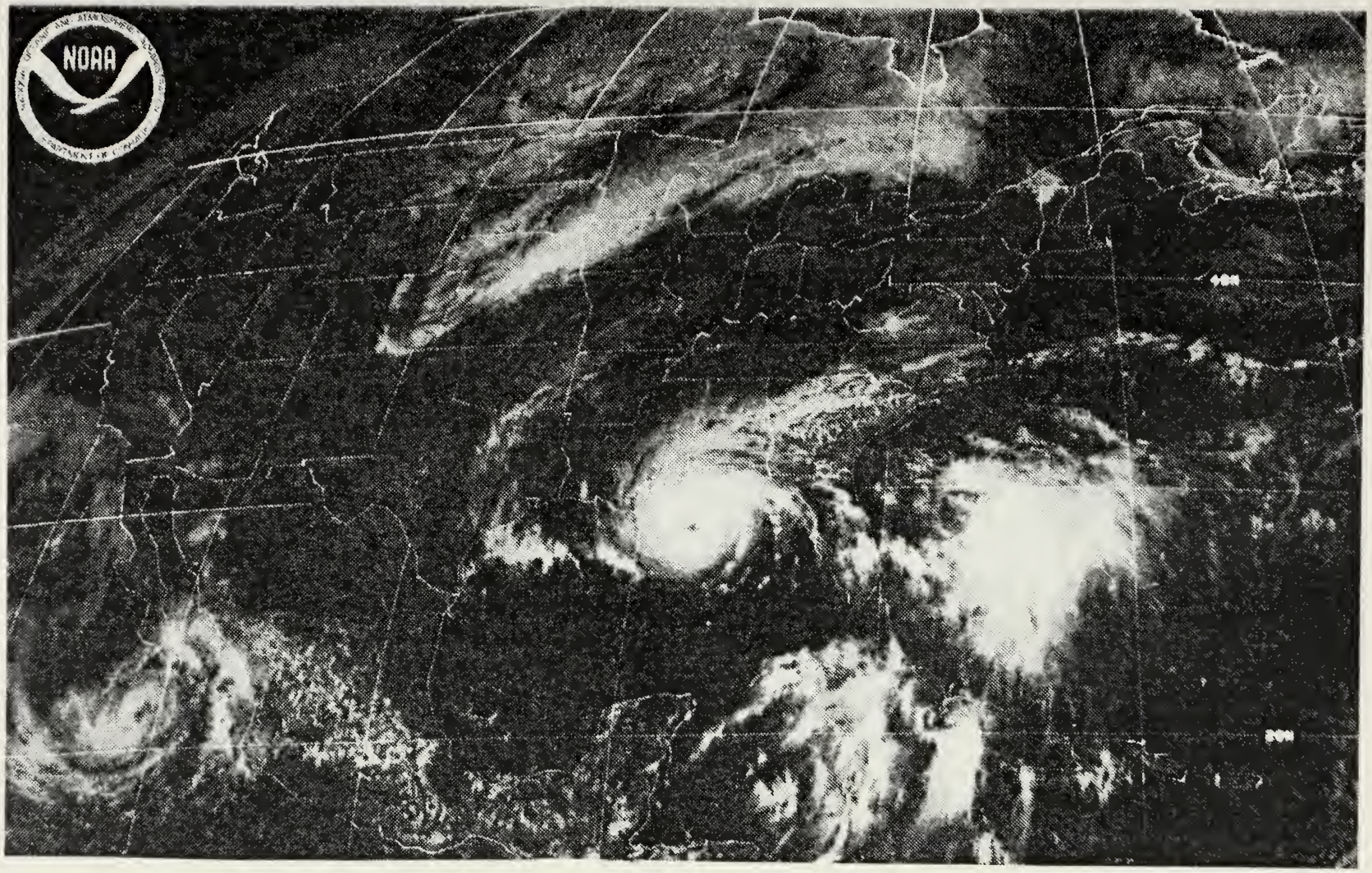

Figure 2. U.S. cloud cover, 1700 GMT 12 September 1979, NOAA satellite photograph, National Environmental Satellite Service.

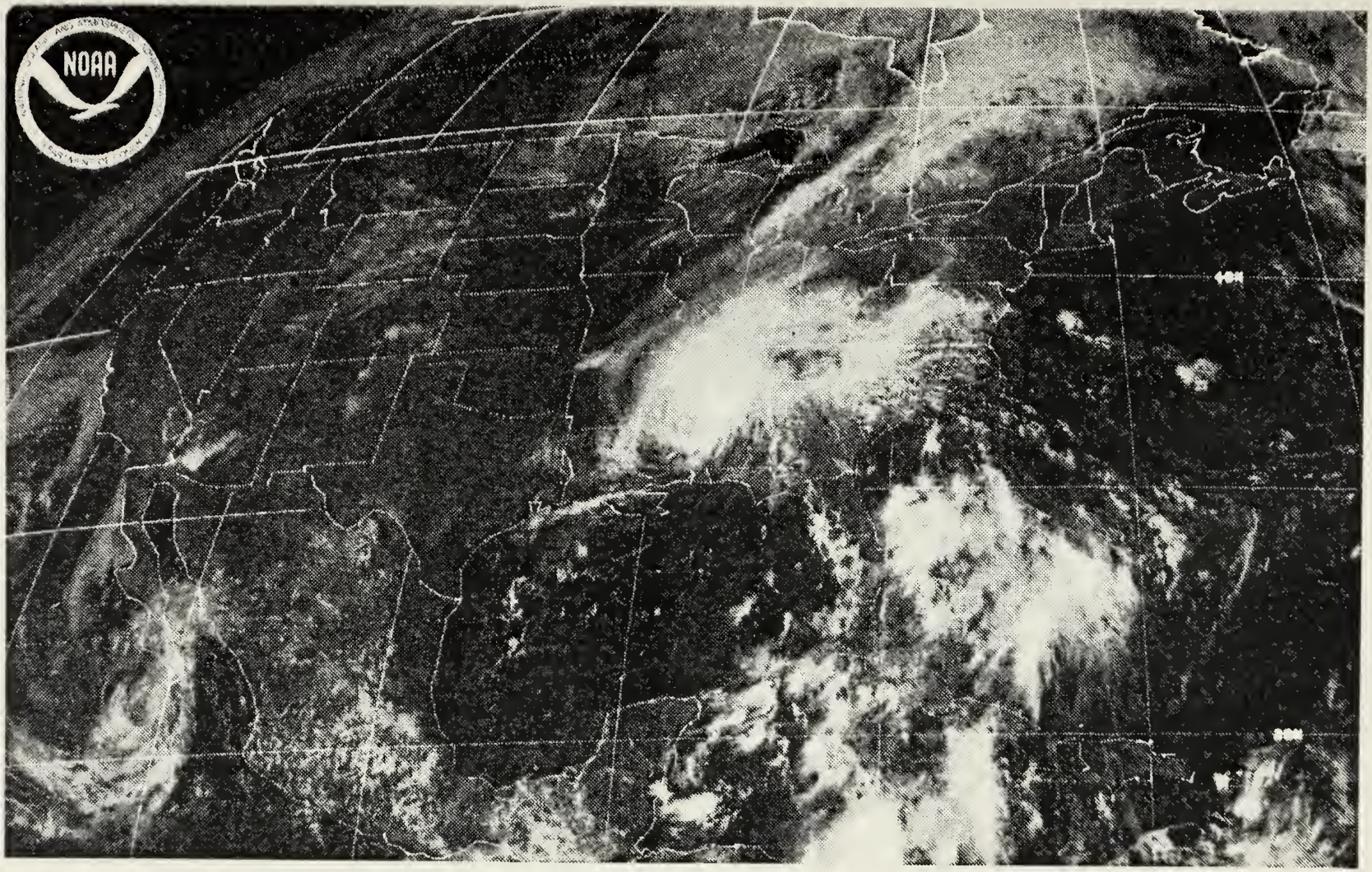

Figure 3. U.S. cloud cover, 1700 GMT 13 September 1979, NOAA satellite photograph, National Environmental Satellite Service.

II. DATA PROCEDURES AND RESULTS

A. BACKGROUND

Ten current meter array records collected at three sites on the continental shelf of the southeastern United States (Fig. 4) during the passage of Hurricane Frederic were provided by NAVOCEANO. As depicted in Fig. 5, the arrays consisted of Aanderaa spar buoys anchored to the bottom. The anchor cable held instruments at three depths at each of the stations one and two and at four depths at station three. The shallowest instrument depth was 19 m at station two, while the deepest was 457 m at station three. The bathymetry (Fig. 5) shows all three stations are on the continental shelf. Data were provided for a continuous period from a few days before the storm passage, about 2100 Greenwich Mean Time (GMT) 12 September 1979, until a few days after the storm passage.

Water depth at station one is only about 100 meters. Price (1981) reported difficulties with meters in a similar coastal environment because of the presence of very strong horizontal gradients and strong topographic effects on the

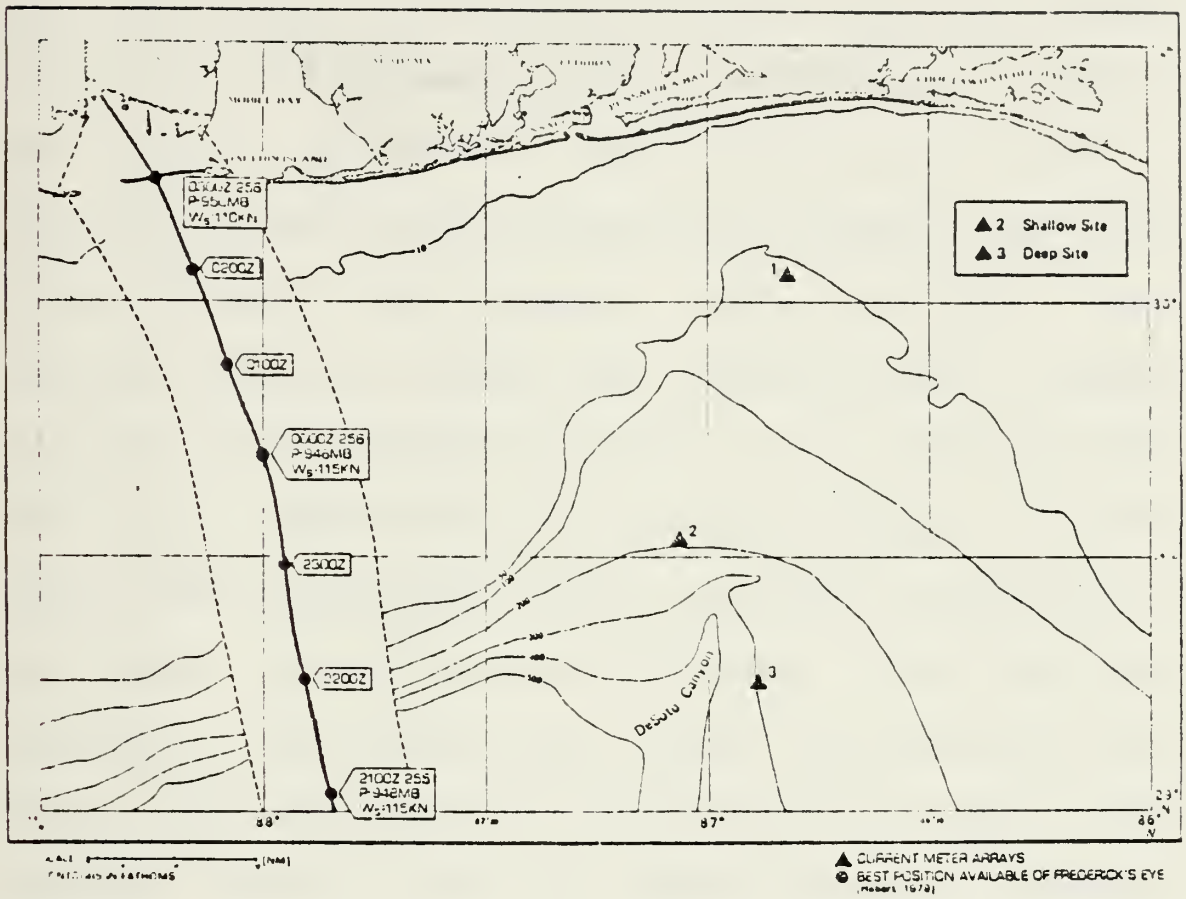

Figure 4. Best position track of Hurricane Frederic and positions of current meter arrays (provided by L.K. Shay, NAVOCEANO).

currents. Mayer et al reported intense, first-mode, near-inertial period oscillations in water of about 70 meter depth. Similar observations at sites in shallower water of about 50 meter depth resulted in only weak, heavily damped, second-mode oscillations.

The current meter records used in this thesis also show a variation in response among the stations with different

bottom depths. At station three where the water depth is about 465 meters, an increase in current magnitude starting about 1920 GMT 12 September 1979 is very apparent in the raw data record (Fig. 6a). This record also shows an oscillation which cycles through one wavelength about once every 24 hours (1440 minutes). This oscillation decays smoothly over about a week, and at first glance it appears to have a period of about 22 hours. A more detailed analysis of the record shows the zero down-crossings to be very nearly 1450 minutes apart during the largest oscillation in the record. The average period for seven cycles during this interval is 1430 minutes (23.8 hours) between down-crossings. The local inertial period at station three is 1473 minutes. Shortly after the surface response, the rapid increase in current magnitude is also obvious at the depth of 457 meters at station three (see Fig. 6b). The average period of the oscillation at this greater depth, 1370 minutes or 22.8 hours, is less than the period near the surface, but the damping of the oscillation is not obvious at 457 meters. At station one where the bottom depth is only about 100 meters, the increase in current speed is detectable in the raw data record near the surface (Fig. 7a), but

any period of oscillation on the order of 24 hours or a damping rate is difficult to detect. An increase in current velocity on 12 September 1979 near the bottom at station one (Fig. 7b) is not apparent and it can be seen that current magnitudes are larger on 9 September than they are on 12 September.

To determine if the observed currents were extraordinary, some idea of the likely currents in the area of observations is helpful. A dominant feature of the Gulf of Mexico surface currents is the Loop Current (Fig. 8). This is a clockwise current of about 50 to 200 cm s^{-1} and 90 to 150 km width (Leipper, 1970) which enters the Gulf in the west as the Yucatan Current, and exits through the Florida Straits as part of the Gulf Stream system. The Yucatan Current flows north from Honduras between the Yucatan Peninsula and Cuba into the central east Gulf and forms the western section of the Loop. Further north the current flows east, southeast, and east again. Elsewhere in the northeastern Gulf, the surface flow is generally cyclonic along the coast until turning southward near Louisiana. Eddies are known to have detached from the Loop Current (Leipper, 1970) and could move into the area of the

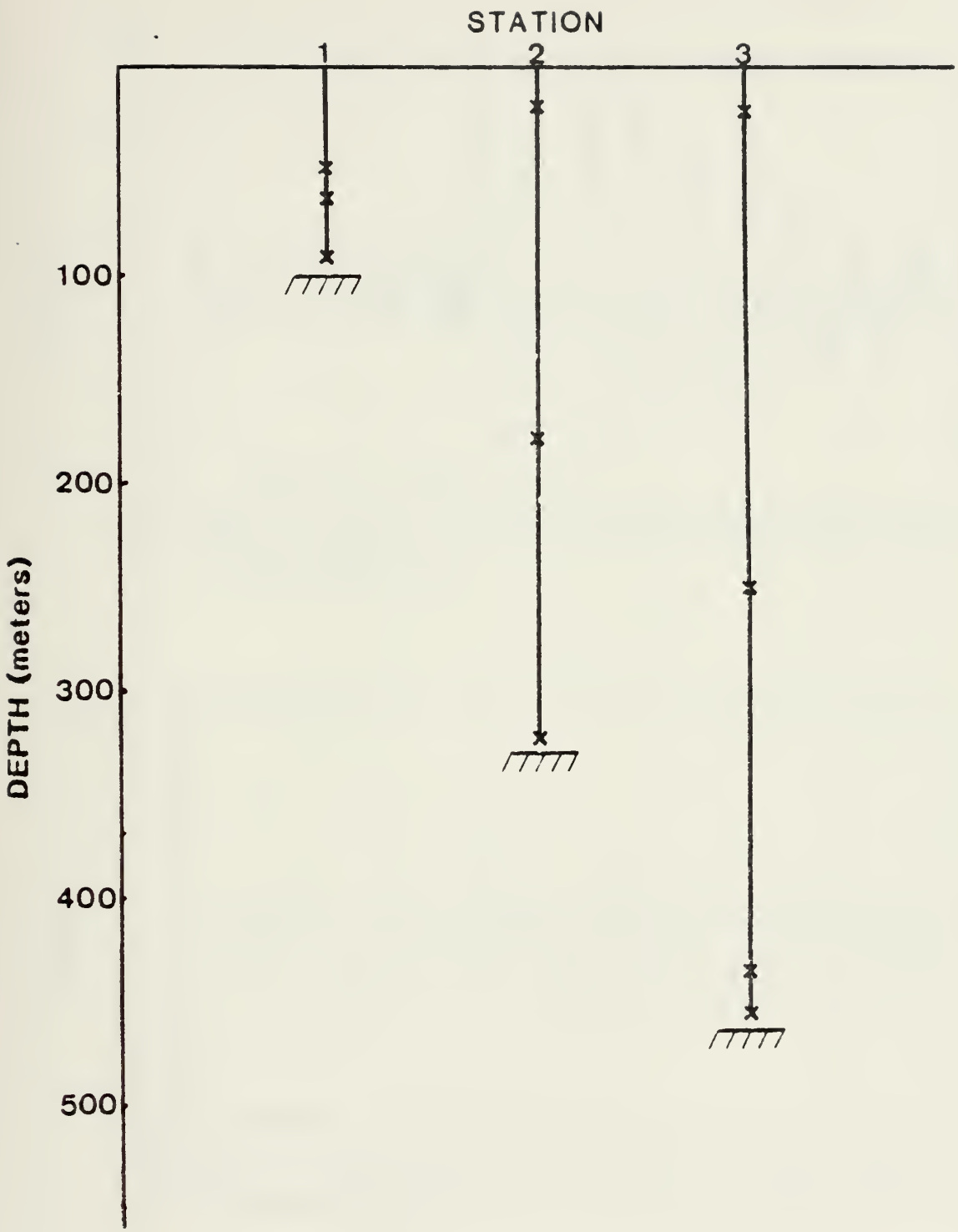

Figure 5. Current meter positions and bottom depths at current meter array sites 1, 2, and 3.

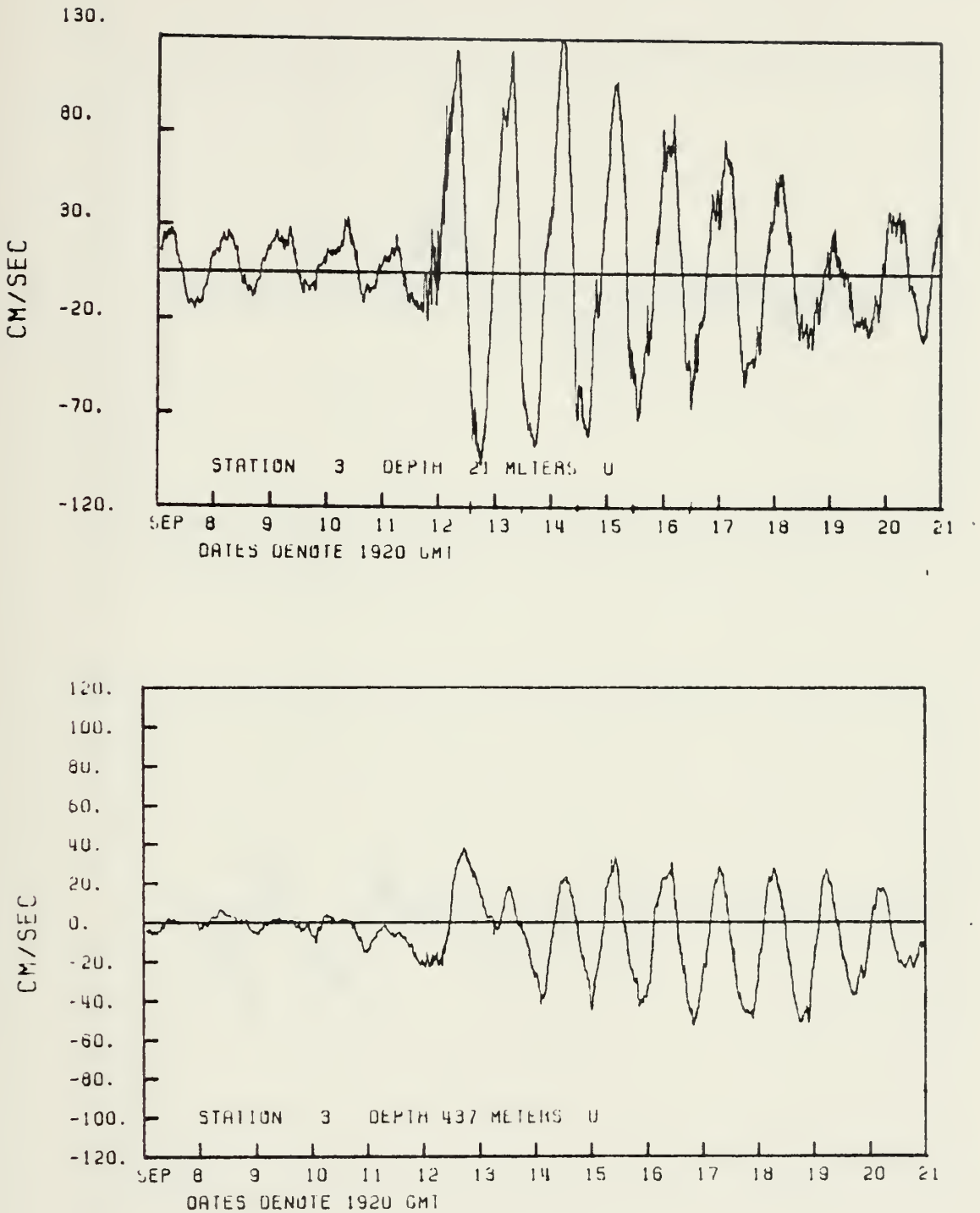

Figure 6. U components of the raw current meter records for 7-21 September at depths of (a) 21 m and (b) 457 m at station 3.

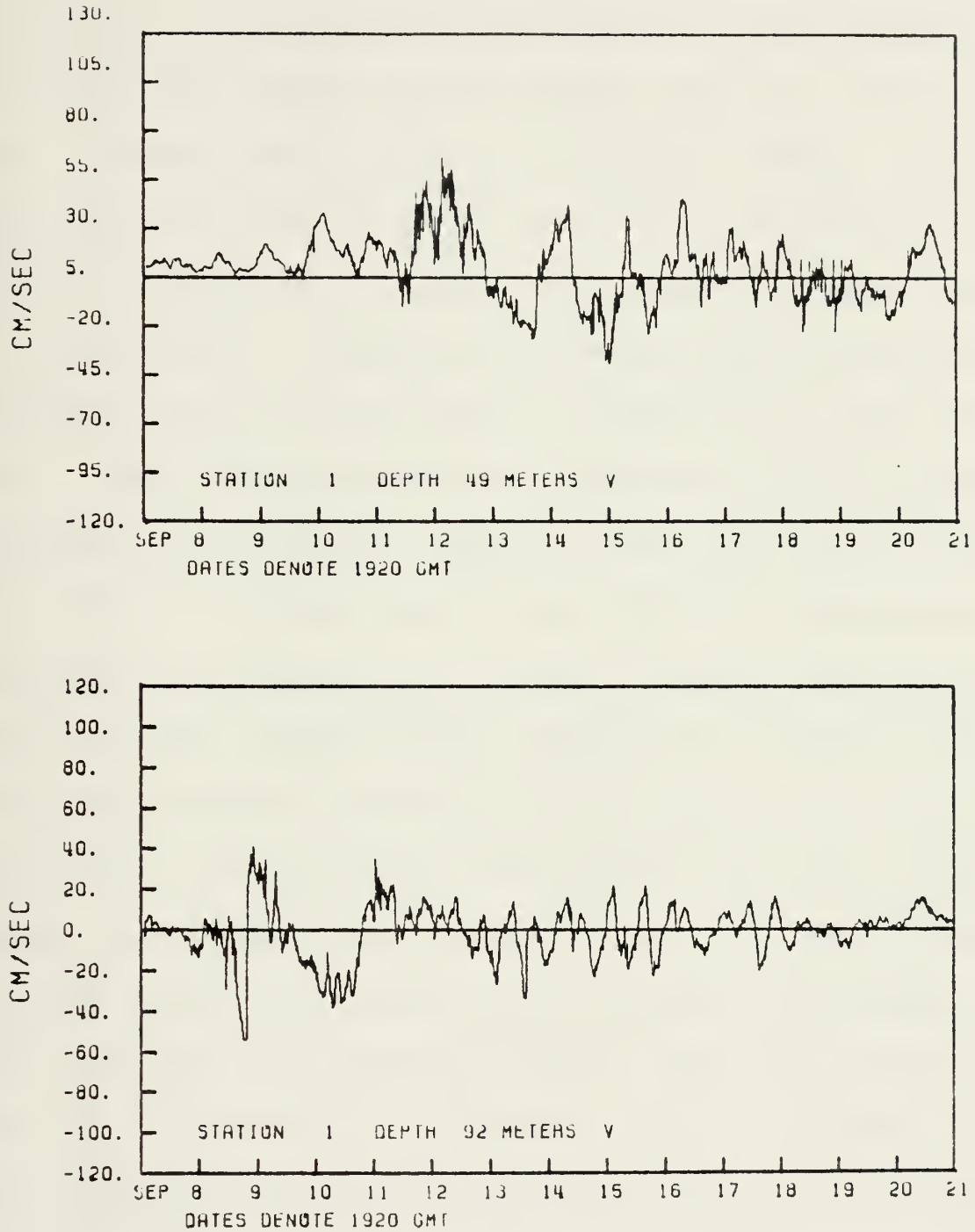

Figure 7. V components of the raw current meter record for 7-21 September at depths of (a) 49 m and (b) 92 m at station 1.

instrument arrays. Leipper (1970) shows a systematic development and breakdown of the Loop Current which places the northern edge of the current further north in the spring than in other seasons (Fig. 9). Molinari (1978) suggests the northward intrusion of the Loop Current is not seasonal, but that climatological results are biased by temporal sampling techniques. Hurlburt and Thompson (1980) presented a numerical study of Loop Current intrusions and eddy shedding. They obtained theoretical expressions for the eddy diameter and penetration distance of the Loop Current into the Gulf and concluded that if only vorticity dynamics are considered, the interaction between the Florida Shelf topography and the pressure field results in a balance which stops the northward penetration of the Loop Current. All of the current array stations are further north than 29 deg North, and although the waters of the Loop rarely extend this far north, Huh et al (1981) examined an intrusion of Loop waters as far north as the data buoys which collected the raw data used in this thesis. It is not possible to tell a priori whether or not the Loop current is in the area of the current meter arrays during the period of observations, but it seems unlikely.

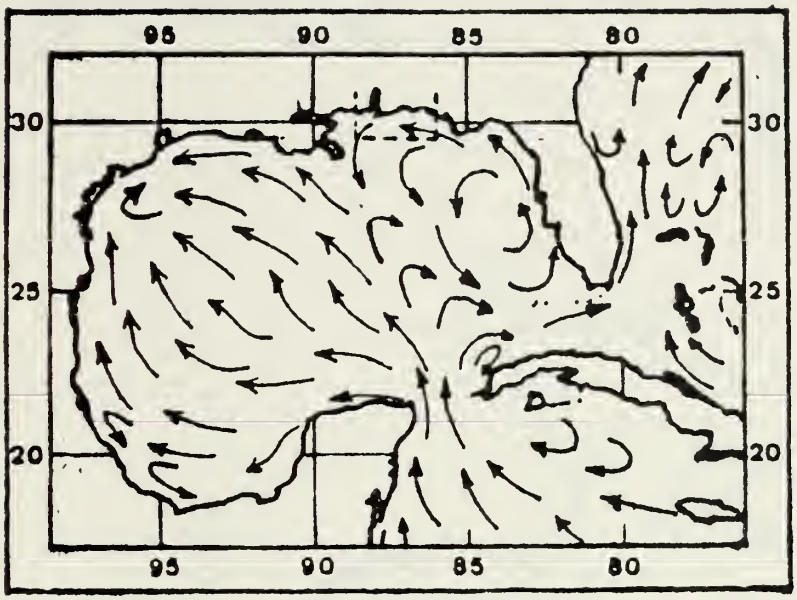

Figure 8. Typical surface currents in the Gulf of Mexico for the months of July, August, September. The general location of the buoy arrays is indicated by the box. (U.S. Navy, 1965).

Another factor which might be expected is the influence of topography. The principle of conservation of potential vorticity causes the current to follow the bathymetric contours. The proximity of the buoys to the coast suggests that near-shore property gradients between the shelf water and the deep water may have important dynamic and thermodynamic consequences. The DeSoto Canyon is also in the area of observations and may tend to enhance cross-shelf circulation.

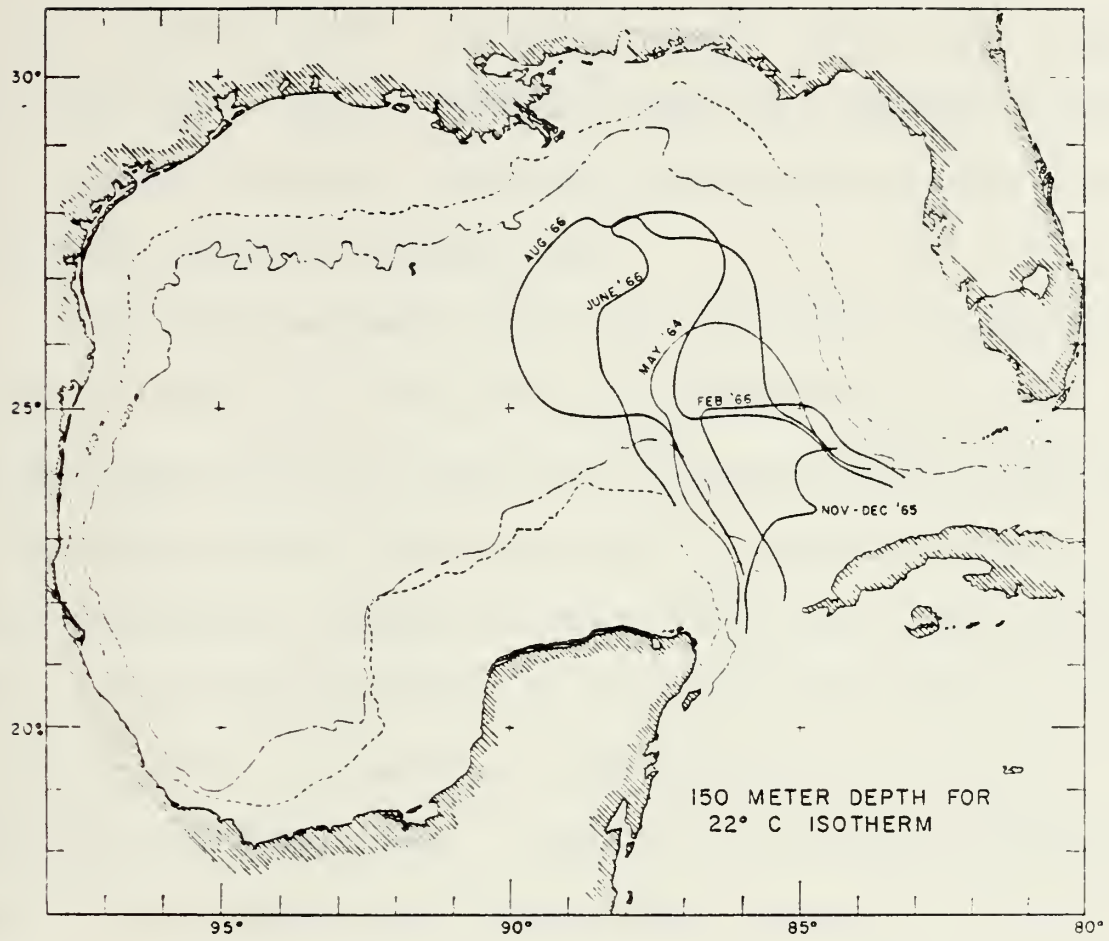

Figure 9. The spring intrusion of 1966 as indicated by overlays of the 150-meter contour lines from the 22°C topographies of all spring cruises of 1966. May 1964 and November and December 1965 are included for supplemental information (Leipper, 1970).

B. RAW DATA

The NAVOCEANO data consisted of north-south (v) and east-west (u) velocity components and temperature (T) at 10 minute intervals. Temperatures above 21.5 °C were not recorded due to thermistor limitations. Temperatures above

21.5 °C occurred only near the surface and complete temperature records were available only from the deeper instruments. Also, NAVOCEANO reported apparent internal clock synchronization problems in the current meter record at 64 meters depth, station one.

The hurricane passed the data buoys with a translation speed of about 7.5 m s^{-1}, and as depicted in Fig. 4, the eye passed about 100 km to the west of station three at 2200 GMT 12 September 1979 (Julian day 255). Maximum winds of 115 kts occurred at a radius of about 30 km from the storm center. The inertial periods for the data buoy locations range from 23 hours, 57 minutes at station one to 24 hours, 33 minutes at station three. That is, the inertial period at all of the stations is approximately one day. Since the diurnal tidal period is 24.8 hours and the semi-diurnal tidal period is 12.4 hours, difficulties could arise in separating any inertial motion from tidal motion before the storm arrival. A spectral analysis would most likely not have sufficient resolution to separate inertial and diurnal motion. The first harmonic of the inertial frequency would also be indistinguishable from the semi-diurnal tidal frequency. However, the large increase in currents, and thus

kinetic energy, observable in the raw data records would be easily detected in an energy spectrum.

The initial data records provided by NAVOCEANO span non-coincident periods. However, all records contained data from 1920 GMT 07 September 1979 to 1820 GMT 21 September 1979. The raw data records (Figs. 6 and 7) show an obvious response to the hurricane forcing starting about 12 September 1979. This hurricane forcing results in increased currents, with maximum values of 130 cm s^{-1} near the surface. Comparison of Figs. 6a and 6b shows that the forcing response was transmitted as deep as 457 meters in less than one half an inertial period. The response to hurricane passage is more difficult to detect in most of the raw data records of stations one and two and it is therefore not possible to estimate the rate at which the response is vertically propagated with depth merely by looking at the raw data record. The ability to detect the increase of energy associated with storm passage at any station and at any level is discussed in the section titled "Procedures for determining relative energies". Although this thesis does not analyze the temperature records directly, the response to hurricane passage is also apparent in the temperature

record (Fig. 10). The temperature record shows an oscillation in the thermocline and an apparent cooling at the 437 m depth at station three, followed by a gradual warming to the end of the period.

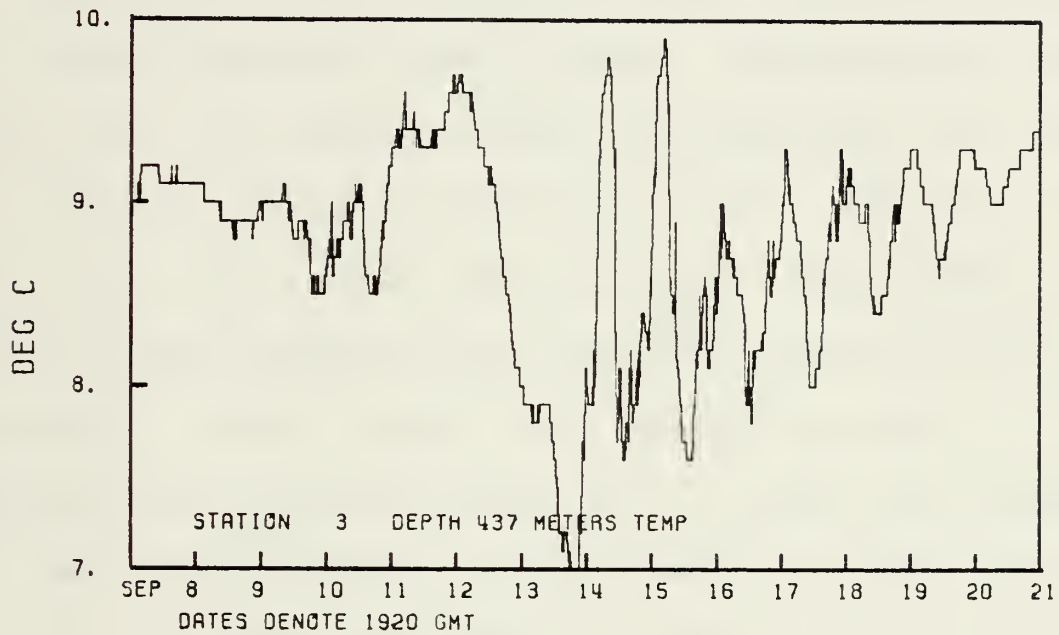

Figure 10. Raw temperature record for 7-21 September 1979 at a depth of 437 m at station 3.

C. DATA MANIPULATION

The initial records were shortened to include only the period 1920 GMT 7 September 1979 to 1820 GMT 18 September 1979. This period was the longest possible period included by all records and was a logical choice since the hurricane eye passed all three buoys between 2100 GMT 12 September and

0300 GMT 13 September 1979. By examining plots of the data (e.g. Figs. 6 and 7) it was determined that significant storm effects with some pre-storm and some post-storm data would be included in the shortened record.

Progressive vector diagrams (PVD's) were plotted for each record during the above period. These diagrams indicated that the inertial motion was superposed on a mean current which was quite different at each location. The mean current was not of primary interest and attempts were made to remove the mean current from the records so that the magnitude, damping period, and associated energy of the inertial motion could be determined. In the first attempt, the mean current over the first three inertial periods (pre-storm passage) was subtracted from all of the u velocity components and the v velocity components. The three inertial period average started at 1920 GMT 07 September, which is five days before the storm center passed the nearest buoy. Comparison of the initial PVD's (Fig. 11) and similar diagrams of the same data with the three inertial period average removed (Fig. 12) was made.

The initial PVD's indicate a general transport in directions which, in most cases, are nearly the same before and

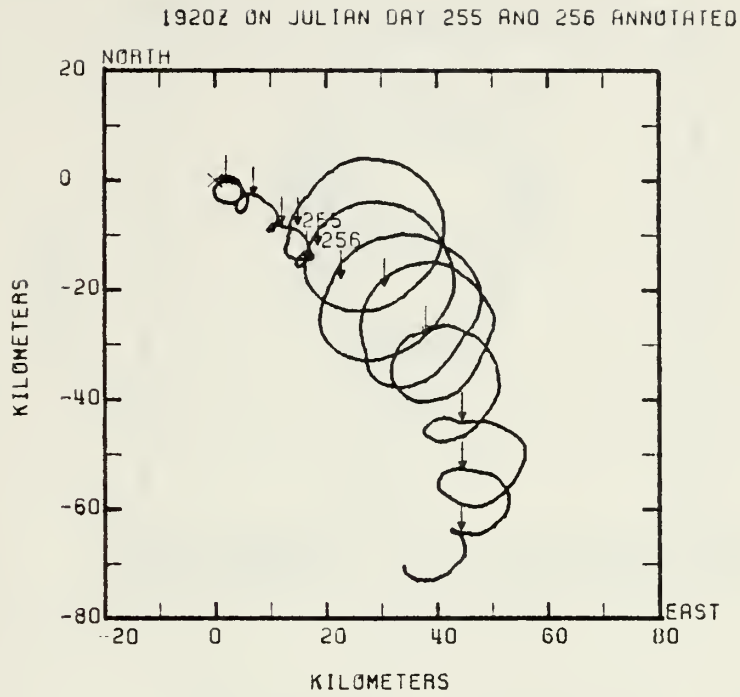

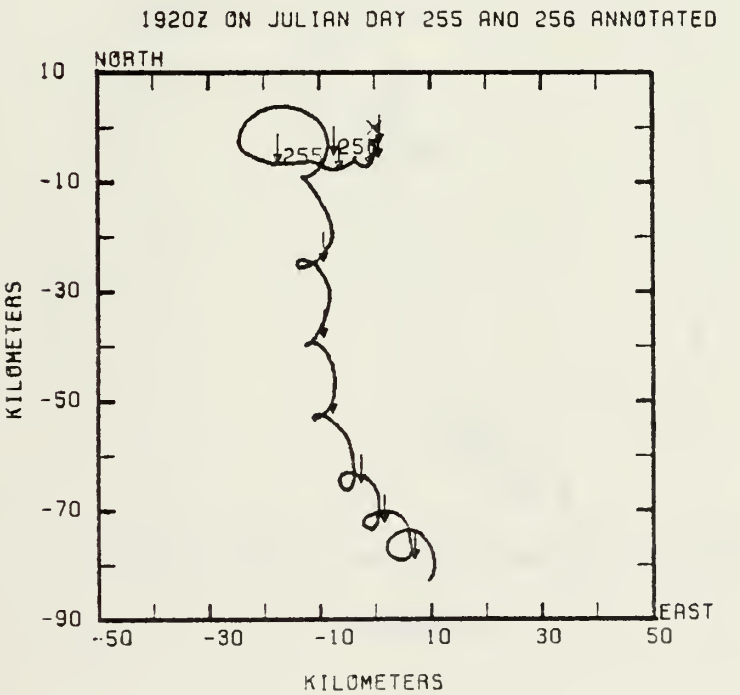

Figure 11. Initial PVD's for 7-18 September at depths of (a) 21 m and (b) 251 m at station 3. The initial location is at (0,0).

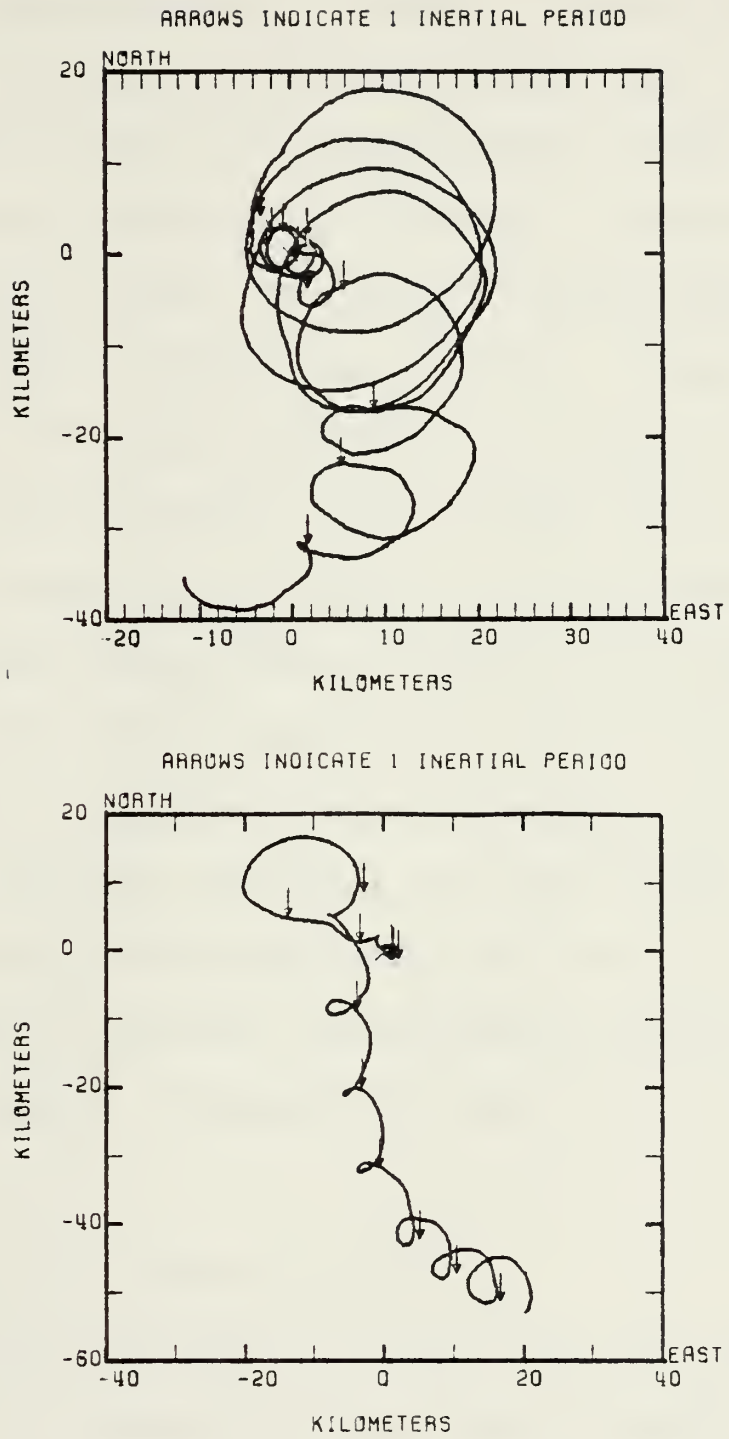

Figure 12. PVD's resulting from the removal of the pre-storm averages over three inertial periods from the PVD's of Fig. 11.

after the storm-induced perturbation. The perturbations are generally reminiscent of inertial motion, i.e. oscillations with a period equal to the local inertial period. PVD's of purely inertial motion would transcribe a simple circle for each inertial period. The circles would overlap if more than one inertial period were plotted. Where the first three days of a record were similar to the mean flow, removing the three inertial period average from the record resulted in more nearly overlapping circular PVD's. Removing the three inertial period average was not effective in isolating the inertial component of the flow when the first three days of the record were not obviously in the general transport direction. Therefore, the mean current was changing significantly during/following the storm at many of the current meter locations. A more effective method of isolating the inertial component from each of the records was required.

D. ISOLATING THE INERTIAL MOTION

In a further attempt to isolate the large inertial component that was obvious in the original records, a running average over the inertial period was computed each three hours and then subtracted from the initial PVD records. The

averaging technique is necessarily applied at the central point of each inertial period, and as a result the half-periods at the beginning and end of the records were lost. However, the transient response is not great at these times and the information lost is inconsequential. Next, the average inertial period record is linearly interpolated between 3-h values to obtain the same number of data points as the initial PVD data. PVD's of the running inertial period average data (e.g. Fig. 13) show that the majority of the inertial flow in the raw data is removed by the running average. The running inertial period averaged PVD's show the general transport direction as well as some features which should be noticeable in a model of the ocean response. A surge to the northeast, onshore, is noticeable in the record of Fig. 13a, and there is some indication that the post-storm current is greater than pre-storm, i.e. the horizontal displacement between inertial period marks is greater after the storm surge than before. The best example of these features in any of the records is shown in Fig. 13b. A surge to the west followed by a counterclockwise loop back into the pre-storm flow direction is evident. Additionally, the post-storm flow is of much greater magnitude than the

pre-storm flow. These diagrams were obviously a better representation of the mean flow throughout the record than the previously computed three inertial period averages. These PVD's also show that the mean current was indeed influenced by the bottom topography. Comparison of Fig. 4 and representative PVD's at stations one, two and three (Figs. 14 and 15) show that the mean flow follows the bathymetric contours. The current moves rapidly toward the northwest at station one during and for some time following the period of hurricane passage (Fig. 14a). A counterclockwise loop which would be associated with inertial motion is not seen as it is in the station two record (Fig. 14b). Comparison of Figs. 13b and 15 shows the flow is along the contours but in opposite directions at the 251 and the 437 or 457 meter depths. Also, a shoreward surge similar to that at the near-surface level of station three (Fig. 13a) is seen at least one inertial period later near the bottom (Fig. 15). The tendency to return to the pre-storm flow direction is much slower at the near-bottom records and is not complete by the end of the record.

The running inertial-period averages are then subtracted from the initial PVD data point-by-point and PVD's of the

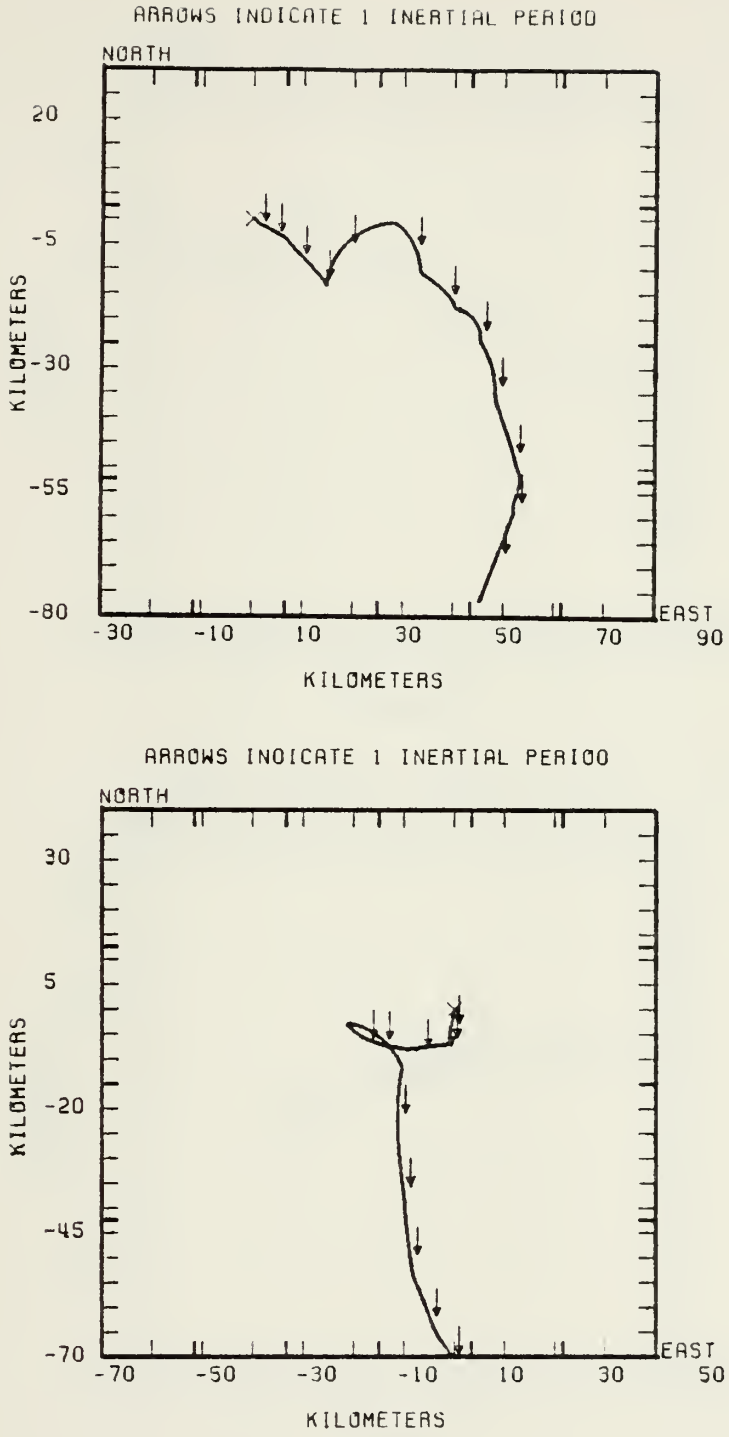

Figure 13. Running inertial period average PVD's for the records shown in Fig. 11. X marks the initial location.

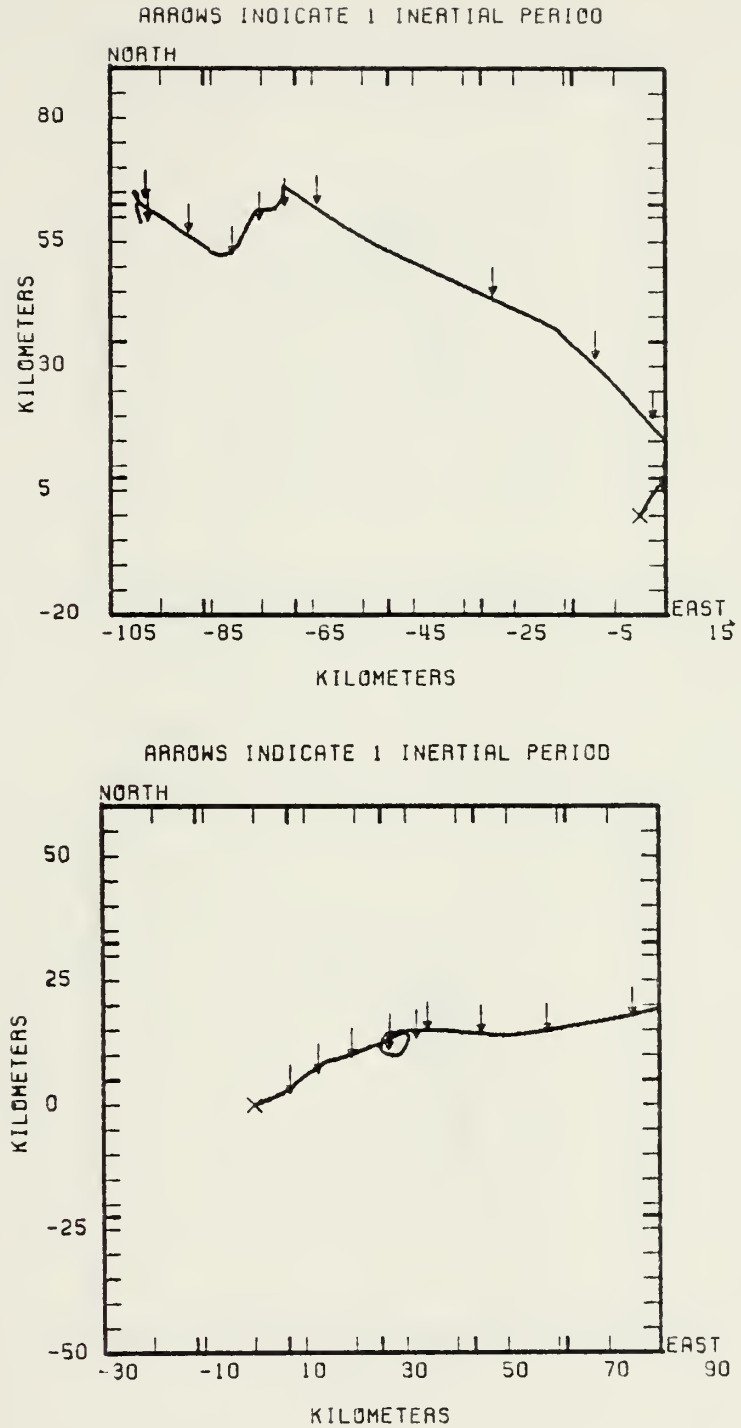

Figure 14. Running inertial period averaged PVD's at (a) a depth of 49 m at station 1 and at (b) a depth of 179 m at station 2.

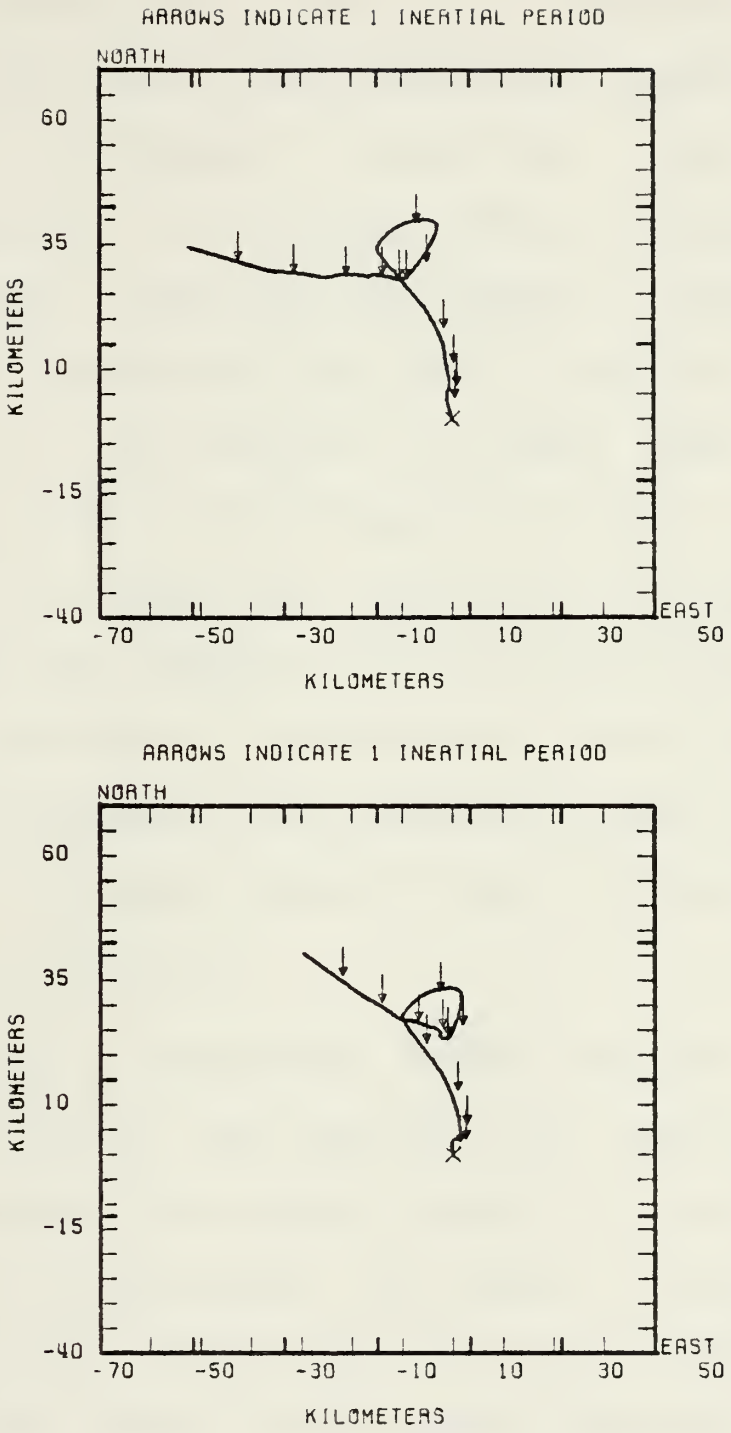

Figure 15. Running inertial period averaged PVD at a depth of (a) 437 m and (b) 457 m at station 3.

resultant data are plotted (Fig. 16). Examination of these resultant PVD's shows that station three exhibits the most obvious inertial response, possibly due to less coastal or bottom influence. The resultant PVD's for stations one and two (not shown) also show large inertial responses. The station one record still exhibits a strong flow which is non-inertial. The station two record shows that the majority of the non-inertial motion is removed.

It is not possible from these plots to determine precisely when the response to the hurricane forcing first begins at each depth. Since the rate at which the energy is transmitted vertically is of interest, the next procedure is to calculate the energy associated with each inertial period at all available levels.

E. PROCEDURES FOR DETERMINING RELATIVE ENERGIES

The PVD's which were computed in the above steps indicate the average of the current record is not zero. Also, a breakdown of these records into inertial periods indicate this nonzero mean current which does exist is not constant throughout the record. An interactive computer program was developed to remove the mean current from a record consisting of inertial flow superposed on a mean current. The mean

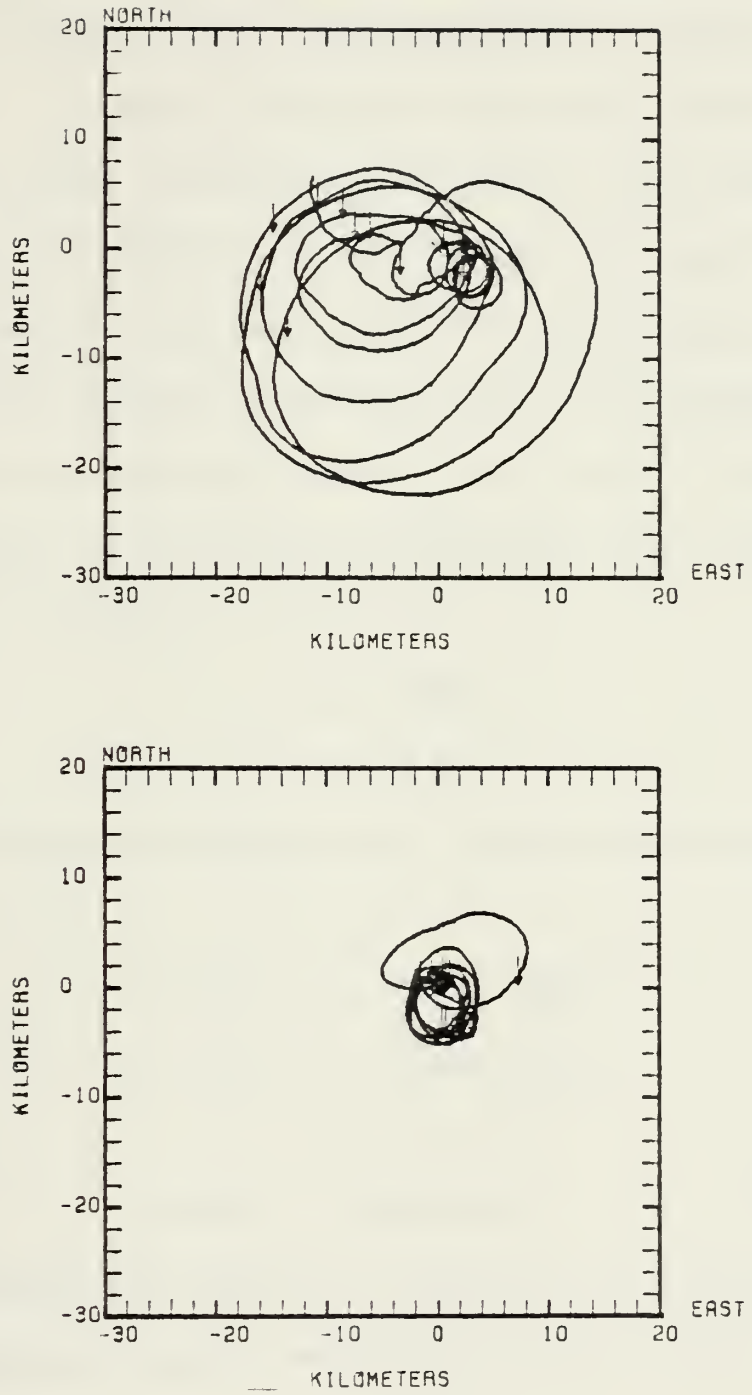

Figure 16. PVD's resulting from the removal of running three-hour averages by inertial period from the PVD's of Fig. 11.

velocity is calculated as the distance between the starting and ending points of the record divided by the duration of the record. An equal portion of this mean current is subtracted from each ten minute interval of the record. The mean current is removed from the record one inertial period at a time rather than for an entire record since the mean current is not constant throughout the entire record.

A circle of radius R was fit to each of the inertial period records. The circle coordinates (x,y) are computed using a mean velocity. Given that

$$x = R \cos(\Theta)$$

$$y = R \sin(\Theta)$$

The mean velocity is computed as the time derivative of the position as:

$$\underline{u} = dx/dt = -R \sin(\Theta)\ d\Theta/dt$$

$$\underline{v} = dy/dt = R \cos(\Theta)\ d\Theta/dt$$

where

$$d\Theta/dt = -2\pi/(N\ dt)$$

and N represents the number of points used to make the circle. Successive x and y coordinates of the circle are then computed as:

$$x1 = x0 + (\underline{u}\ dt)$$

$$y1 = y0 + (\underline{v}\ dt)$$

The starting position is x = 0. and y = -1., i.e. at 270 degrees of a 360 degree circle centered at (0.,0.), and the successive positions are created in a clockwise fashion. The radius of the circle is adjusted using an error minimization program. This program calculates the distances between the positions required to create the circle and the positions used to compute the PVD's, and selects the circle which gives the smallest sum of positional distances. One fourth of the maximum dimension of the plotted data is used as the initial radius for the minimization subroutine. While the radius is held constant, the sum of the difference between an "average error" and an "individual position error" is computed and divided by the number of differences. This error difference is used in the following calculations. The distances between all points of the computed circle and the data are first compared to locate the data point and the circle point which are closest. These points are used as the starting positions for the distance error computations. The "average error" is the average of the distances between the consecutive points of the data and the computed circle. The "individual position error" is the distance between a point on the circle and a data point. The error difference

for one radius is stored and, the radius is slowly incremented to twice the original magnitude, storing the error difference at each increment. The radius corresponding to the minimum value of error difference is used to create the circle which best fits the plotted data.

The circle created using this adjusted radius is used as the best fit. It is then possible to estimate the energy per unit mass associated with each inertial period. The inertial velocity (V=fR) associated with the circle radius R and coriolis parameter f is computed. One half of the square of this velocity is assumed to be the energy per unit mass. The circle fitting error difference computed as above is divided by the radius of the fitted circle and referred to as the relative RMS error. The energy values are plotted versus the inertial period at each level at each station (See Figs. 17 and 18). The radius for each inertial period, the relative RMS error of fitting the circle and the mean current removed from each inertial period are listed in Table II for the records from station one at a depth of 49 m and from station three at a depth of 21 m. Also, the minimization program is tested using exact circles as input data. The resultant errors for given radii are also listed

in Table II. The exact circle error shows the error is near zero when the motion is circular. The error is found to be a smaller percentage of the radius, i.e. the relative RMS error is smaller, at station three than at station one. This supports the previous results of the motion being more nearly circular, and thus more inertial, at station three than at station one.

A good fit between the positions of the generated circle and the positions from the real data with the inertial mean removed is obtained for the records of station three where the water is deepest and the coastal influence is least (Fig. 19a). The agreement in positions between the two curves at station one is generally less since these records are affected more by the bottom, and by tidal motion which is not necessarily removed. Obviously non-inertial motion remained in the station one record (Fig. 19b). Example plots of the record after all means were removed are shown in Fig. 20. The figures show nearly overlapping circular motion except for different radii. Plots of the energy values versus inertial periods are given in Fig. 17 for the level nearest the surface at each of the three stations. Energy values of 4000 at station 3 correspond to an

TABLE II

Example circle radii, relative RMS error and mean current removed for each inertial period and for an exact circle

STATION	INERTIAL PERIOD	RELATIVE RMS ERROR (km)	CIRCLE RADIUS (km)	CURRENT REMOVED (cm s^{-1}) u	v
1	1	.3505	.321	- .13	.04
	2	.3775	.631	- .39	- .56
	3	.3810	.839	-5.18	.38
	4	.2622	1.152	1.15	1.69
	5	.1668	2.663	-6.53	1.33
	6	.1688	2.602	- .52	2.03
	7	.1370	2.859	6.18	-10.77
	8	.1580	2.577	1.22	2.44
	9	.2110	1.128	.24	.43
	10	.2219	1.560	-3.23	4.73
	11	.2165	1.714	1.16	-2.62
	12	.2695	1.302	2.89	-1.64
3	1	.0818	2.547	- .01	.29
	2	.0738	2.335	1.83	- .29
	3	.1501	2.106	.19	-1.17
	4	.1530	2.035	.20	- .92
	5	.2813	1.440	-5.67	2.92
	6	.0339	12.455	-9.66	-2.81
	7	.0322	12.116	-1.83	5.89
	8	.0160	13.394	3.52	4.75
	9	.0316	10.904	3.56	- .16
	10	.0301	6.357	2.07	3.77
	11	.0583	5.818	- .67	.89
	12	.0858	3.891	-2.00	-2.16
True Circle		.0033	.300		
		.0022	.500		
		.0002	1.000		
		.0003	2.000		
		.0002	3.000		
		.0005	4.000		
		.0023	8.000		
		.0002	16.000		
		.0021	30.000		

amplitude of the inertial current of about 90 cm s^{-1}. The energy values at station one are much smaller than those at station two and three. The technique employed to fit the

true circle to the manipulated data accounts for some of this difference. When the data points are not circular, the circle is adjusted to some value less than the largest dimension of the plotted data. When the data form a circle, the largest dimension of the plotted data and the dimension of the circle nearly coincide. For stations two and three, a sharp increase in kinetic energy is indicated in Fig. 17 during the fifth inertial period. These energy values remain high for two to three inertial periods before rapidly decreasing toward the pre-storm levels. Similar plots for the next deepest level at each station are shown in Fig. 18a. At stations one and two the energy peaks rapidly, falls off rapidly and then increases to the end of the record. At station three, a slower increase is noticed, and is followed by a nearly constant value to the end of the record. A slower increase in energy is found (Fig. 18b) at the 437 m and 457 m levels at station three. The energy values do not appear to have peaked by the end of the record. Since the records of Fig. 18 are within 20 m of each other, it would be reasonable to assume the records would be nearly identical. The difference could be due to bottom reflection of energy since the 457 m instrument was

positioned only 8 meters from the bottom. At the very least, the procedures used to determine the energy associated with the inertial motion should produce results accurate to within a factor of two and should also indicate the trends. No confidence is placed in the details of the fluctuating values. However, the large peaks and long term increases shown in the energy records are thought to be significant.

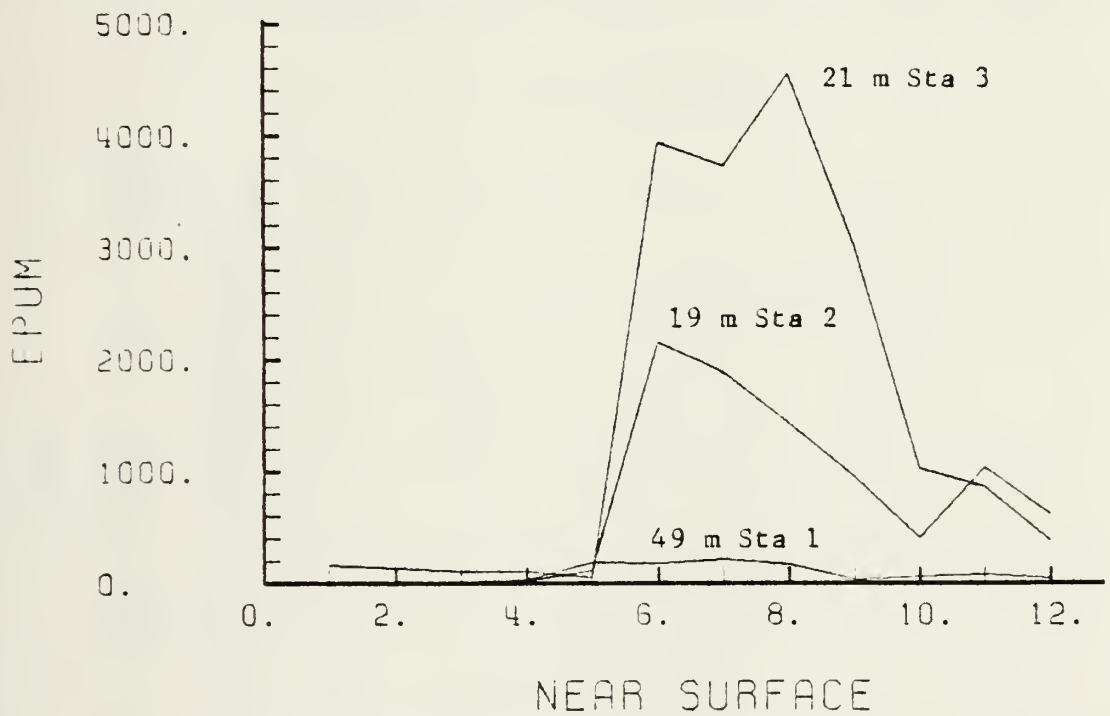

Figure 17. Energy (m^2 s^{-2}) versus inertial period at the near surface levels at stations one, two and three.

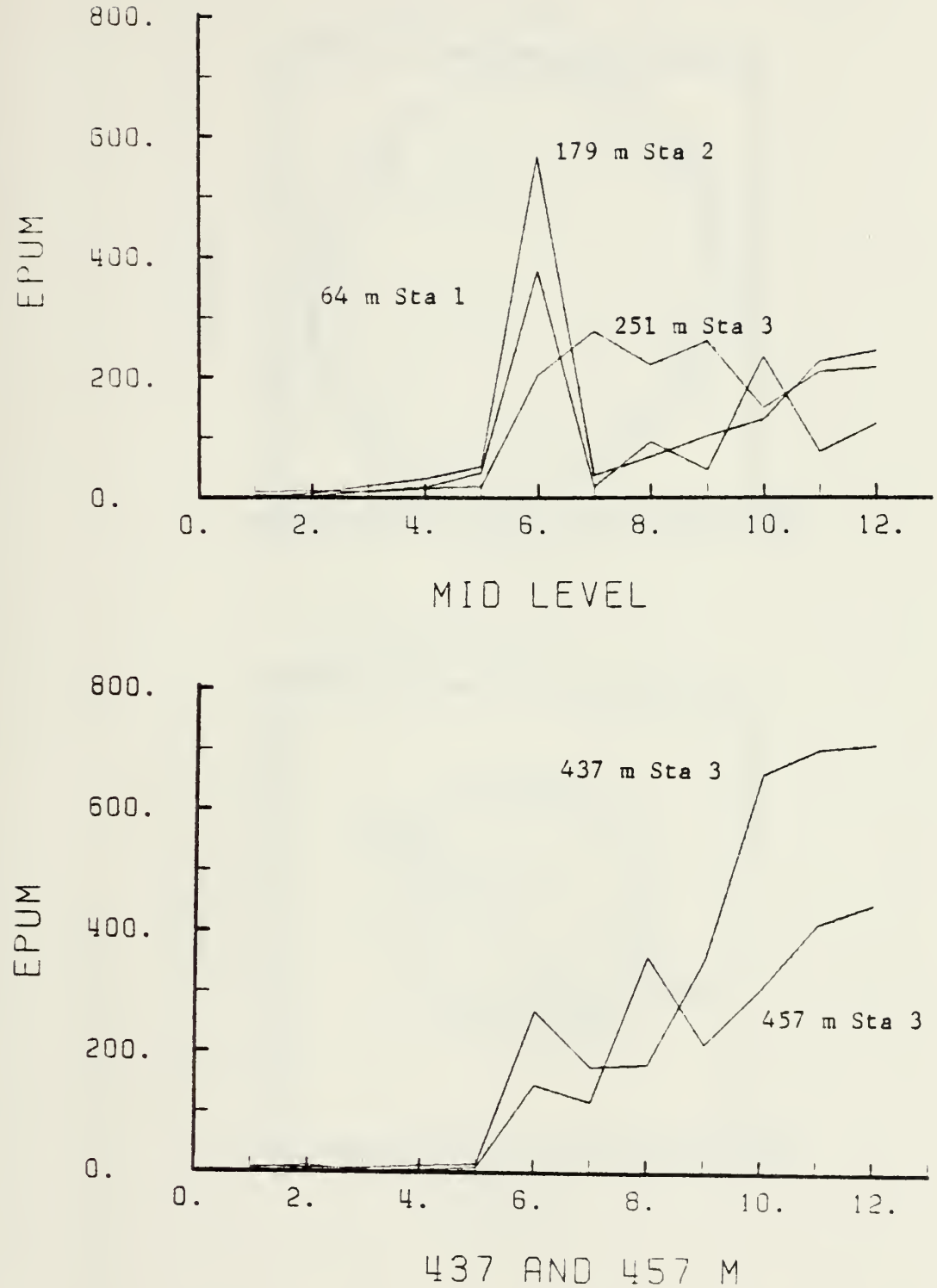

Figure 18. Energy ($m^2 s^{-2}$) versus inertial period at (a) the mid levels of each station and (b) the two bottom levels at station three.

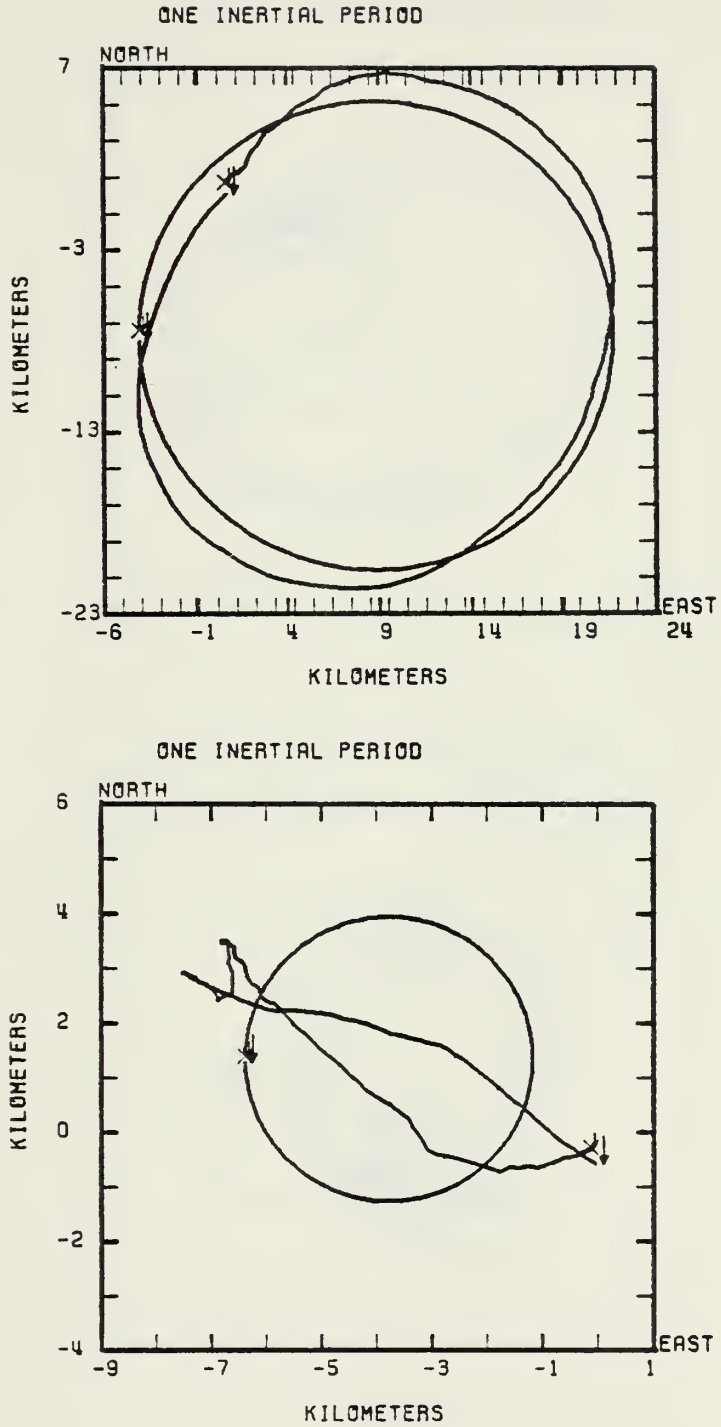

Figure 19. Manipulated real data record and calculated circle for (a) inertial period 6 at station 3 and (b) inertial period 6 at station 1.

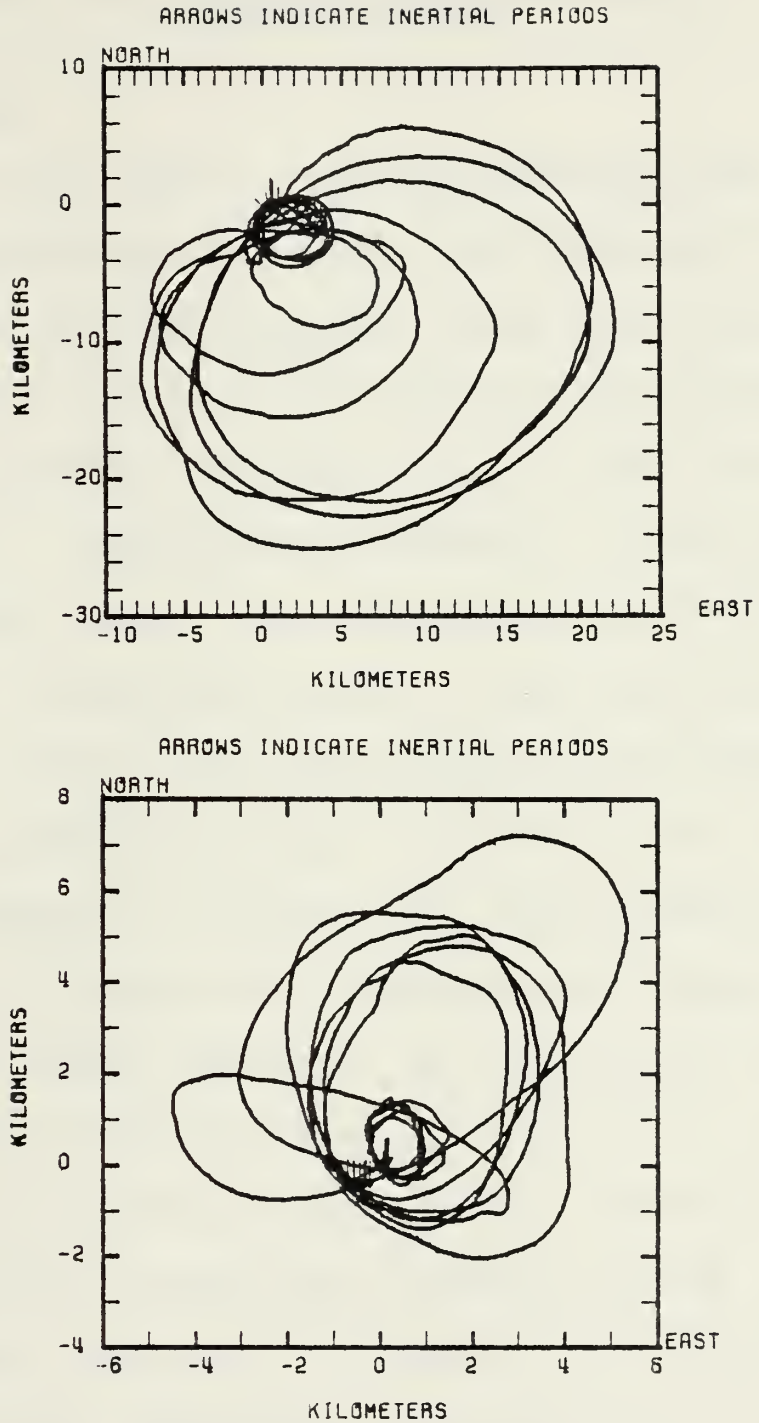

Figure 20. PVD's after removal of mean currents at a depth of (a) 21 m and (b) 251 m at station three.

III. THE EMBEDDED MIXED LAYER--OCEAN CIRCULATION MODEL

A. BACKGROUND

Adamec *et al* (1981) tested an embedded mixed layer-ocean circulation model. This model embedded Garwood's (1977) model for predicting mixed layer depth and jumps in temperature and velocity at the base of the mixed layer in a six-level, primitive equation open-ocean model developed by Haney (1981). These authors remarked in their conclusion that additional tests, "including comparisons with observational data", were being planned. This thesis constitutes an important step in those plans because of the availability of suitable observational data. The model used in the 1981 study is expanded to simulate the three-dimensional ocean response to a translating hurricane-type forcing field. This model forcing represents an axisymmetric hurricane translating at a constant speed of 7.5 m s^{-1}. The model ocean basin is a 960 km square with six layers of varying depth between the surface and a free-slip bottom at 400 m. The horizontal resolution is 15 km on a 65 by 65 grid. The level depths and thicknesses are represented in Fig. 21. The time step used in the 1981 study, 450 s, is increased to

600 s. A brief explanation of the model as used in this thesis is given below.

B. MODEL FORMULATIONS AND BOUNDARY CONDITIONS

The governing equations are the primitive Navier-Stokes equations, the continuity equation, the hydrostatic equation and the equation of state (see Adamec et al, 1981). The hydrostatic assumption is applied, and the ocean is assumed incompressible with density being a linear function of temperature only. The coriolis force varies appropriate to the latitude of the domain from 25°N to 33.6°N. The change in coriolis parameter (f) with latitude is computed as a finite difference at each north-south grid point.

There are no fluxes of mass, momentum or heat across the bottom (flat) or side (vertical) boundaries. Also, the rigid lid approximation ($w = 0$ at $z = 0$) is made, which requires the vertically averaged motion be zero. Applying this approximation to the Navier-Stokes equations provides prediction equations for the vertical shear currents (see Adamec et al, 1981). Vertically averaging the continuity equation over the mixed layer and applying $w = 0$ at $z = 0$ yields a prognostic equation for the vertical velocity at the base of the well-mixed layer, $w(-h)$. The entrainment

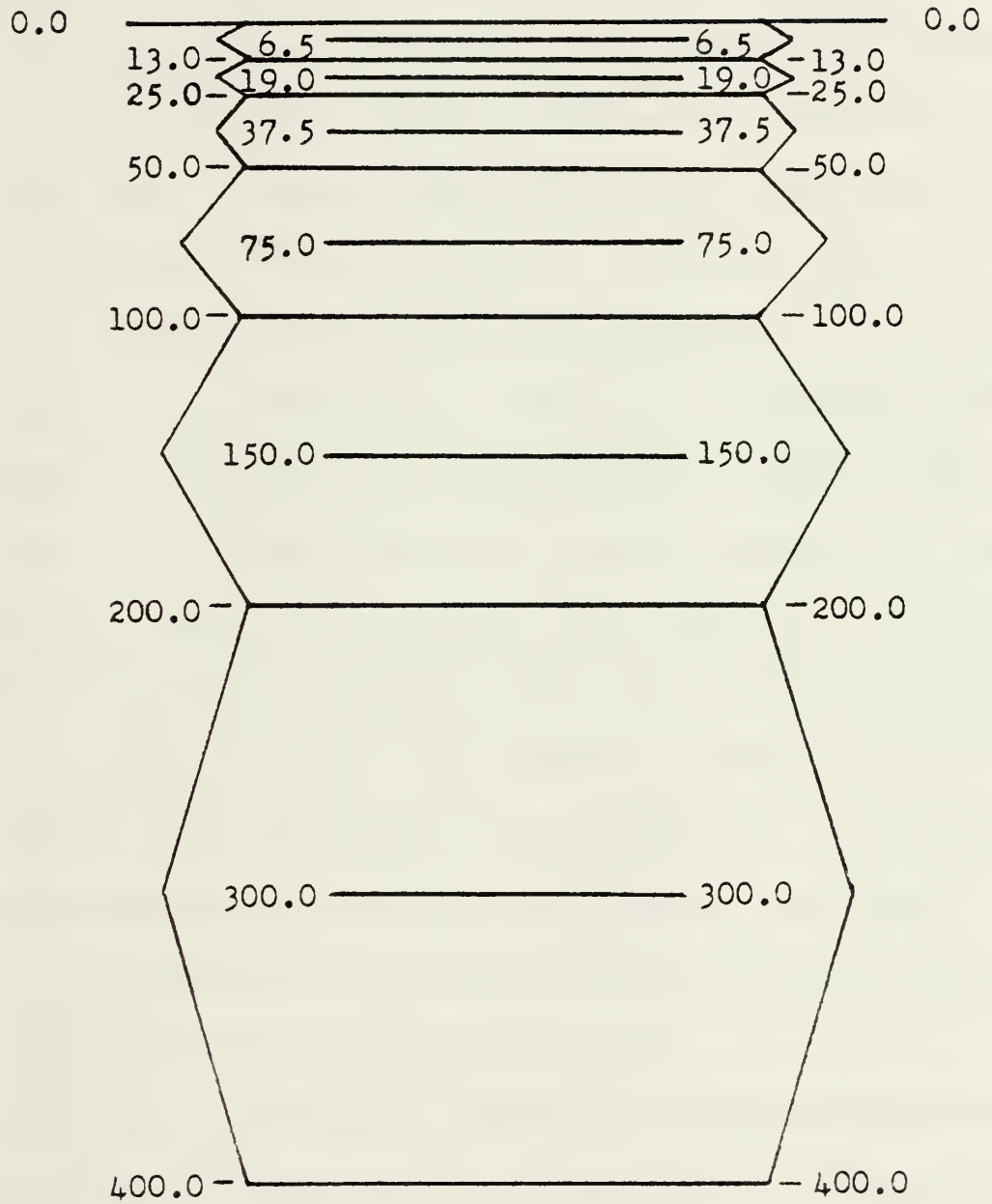

Figure 21. Representation of the six mixed-layer--ocean circulation model layers. Computation levels for $\underline{u}$,$\underline{v}$ and $\underline{T}$ are midpoints noted in each level.

velocity is predicted by the mixed layer model. Together with $\underline{w}(-h)$, this yields a prognostic equation for mixed layer depth.

The axisymmetrical portions of the hurricane forcing are shown in Fig. 22. The tangential and radial stresses are of the same form. They are calculated from a prescribed wind, which increases linearly from the storm eye wall to the radius of maximum winds, and then decreases as $\underline{r}^{-1/2}$ to $\underline{r}$ = 360 km and then linearly to $\underline{r}$ = 450 km. The radius of maximum winds is 45 km and the inner boundary of the eye wall of the storm is 4.5 km. This wind profile results in a wind stress curl which is zero inside the eye wall, increasing linearly from zero at the eye wall to a maximum at 45 km, zero from 45 to 360 km, and negative from 360 km to the boundary of the wind stress (about 450 km). The maximum tangential stress corresponds to a maximum wind speed of 50 m s^{-1}. The small value of radial stress (-12.9 dPa max) is due to cross isobaric flow of about 20°.

Below the mixed layer, vertical diffusion is applied to the momentum or temperature equations with a vertical eddy viscosity or eddy conductivity coefficent (both equal to 0.5 cm s^{-2} at all depths below the surface mixed layer). In the

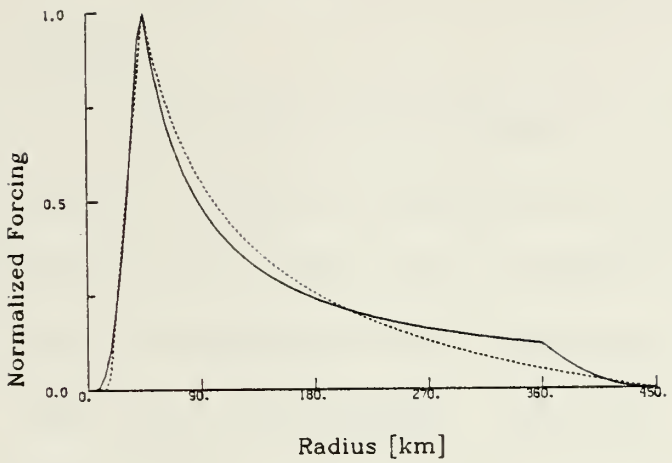

Figure 22. Forcing functions for the ocean model, each normalized by the value of the function at the radius of maximum winds. The tangential and radial stress components have the same form (solid line) with maximum values of 35.9 and -12.9 dPa, respectively. The surface heat flux (dashed) has a maximum value of -840 W m (Adamec et al, 1981).

mixed layer, however, the above formulation is not appropriate. The depth of the mixed layer is the boundary between intense turbulence and the much less turbulent waters beneath.

C. ENTRAINMENT AND MIXED LAYER MODEL FORMULATION

In the mixed layer, prognostic equations for the mixed-layer average (bulk) values of the vertical component of turbulent kinetic energy and the total turbulent kinetic energy are derived using the bulk, second-order closure methods of Garwood (1977). Computation of the entrainment buoyancy flux allows calculation of the downward fluxes of

heat and momentum associated with entrainment at the base of the mixed layer.

The above mixed-layer formulation allows the fraction of turbulent kinetic energy available for mixing at the base of the mixed layer to be other than a constant. This turbulent kinetic energy is diagnostically dependent upon the surface buoyancy flux and the surface friction velocity (known boundary conditions). It is thus possible to couple the diagnostic mixed-layer formulation with the prognostic ocean circulation model in a numerically feasible fashion.

Both increases and decreases in mixed layer depth must be considered in any mixed layer model. The easier of these two events to formulate is the increasing mixed layer depth case. The method requires determination of the entrainment heat flux and then imposing this heat flux on the given temperature profile. Added vertical resolution near the base of the mixed layer is given since the base is not required to coincide with any of the prescribed model levels. This increased vertical resolution is very important since the thermocline profile determines the potential energy of the upper ocean. The dynamics of the mixed layer and the ocean circulation are dependent on this potential energy.

Formation of a new, shallower mixed layer occurs whenever the turbulent mixing is not able to penetrate all the way to the previously established depth of the mixed layer. This layer reformation occurs when warming of the surface layer occurs with no increase in the wind shear to sustain the mixing. Numerical formulation of this event is difficult because the previous structure at the interface can not readily be preserved. Thus energy budget problems may arise when deepening to the prior mixed layer depth does occur. This model uses a numerical procedure (see Adamec et al, 1981) that preserves potential energy to ensure the deepening rate is as correct as possible when the layer again deepens to the earlier mixed layer depth. This feature of the model is not tested here because the solar flux is zero throughout the simulation.

D. DYNAMIC STABILITY CONDITION

It is assumed that the mixed layer is dynamically unstable and the underlying water column is normally dynamically stable. However, dynamic instability of the underlying water column can sometimes occur. In this model, vertical fluxes of heat and momentum between levels are imposed so that the gradient Richardson number remains greater than or

equal to a critical value. This generalization of the more common convective adjustment is referred to by Adamec et al (1981) as "dynamical adjustment".

E. COUPLING OF THE DYNAMICAL AND MIXING PROCESSES IN THE MODEL

The mixed layer and the dynamic portion of the model, which is a level model that predicts the average of a quantity in a layer, are coupled in two phases. First, advective and diffusive changes in the upper ocean are calculated in the dynamic part and put into a form useable by the mixed layer model. Then, the surface flux and entrainment changes are calculated by the mixed layer model and transmitted to the dynamic part of the model. A special treatment of the level which contains the base of the mixed layer is required (see Adamec et al, 1981).

F. COMPARISON OF THE MODEL AND THE DATA

The model provides a four-dimensional space-time view of the ocean response to a moving hurricane. The data provided by NAVOCEANO is two-dimensional, time and depth, at three different stations. All three locations are to the right of the storm track beyond the radius of maximum winds of the storm. The differences in instrument depths and the limited

number of stations do not allow the extension of the data into a third dimension. The comparison of the data and the model, then, is an attempt to:

- compare the general physical characteristics of the model results to see if they are reasonable in light of the observed data results,
- choose a data set from the model which is similar to the raw data in number, depth and location relative to the storm,
- compare this data to the NAVOCEANO data to show whether or not the model is providing a realistic response to the simulated hurricane forcing, and
- examine the four-dimensional model results for characteristic ocean response to hurricane forcing which could not be observed at the data stations.

G. GENERAL CHARACTERISTICS OF THE MODEL

The initial position of the hurricane is at grid point (23,16). Since the grid spacing is 15 km, grid point (23,16) corresponds to a distance in the x direction of 330 km and in the y direction of 225 km. Model output includes north-south and east-west velocity components, $\underline{v}$ and $\underline{u}$; temperature, $\underline{T}$; and mixed layer depth, $\underline{H}$. The initial values of these quanties are given in the following table. The quantities $\underline{u}$, $\underline{v}$, and $\underline{T}$ are extracted at both three hour intervals for the entire grid at all six levels and at ten minute intervals for selected grid points and levels. The mixed layer depth (MLD) is stored at three-hour intervals.

TABLE III

Initial values of model output variables

			T at level					
u	v	H	1	2	3	4	5	6
(cm s^{-1})		(m)			(°C)			
0	0	30.	30.0	29.2	28.1	23.4	18.4	13.1

The results predicted by the model at 36 and 48 h at level 1 are presented in Figs. 23a--d and Figs. 24a--d, respectively. Using the storm translation speed of 7.5 m s^{-1}, the distance of the storm from the bottom of the grid is given in Table IV. The storm center has tracked off the grid by hour 24 and the southern boundary of the storm has passed the edge by hour 48.

TABLE IV

Hurricane distance from bottom of grid at six-hour intervals

DISTANCE	HOUR
330	0
492	6
654	12
816	18
978	24
1140	30
1302	36
1464	42

Several important features are noticeable in Figs. 23 and 24:

- The current fields at 36 and 48 hours are "out of phase", i.e. the areas of westerly currents at hour 36 are generally easterly at hour 48.

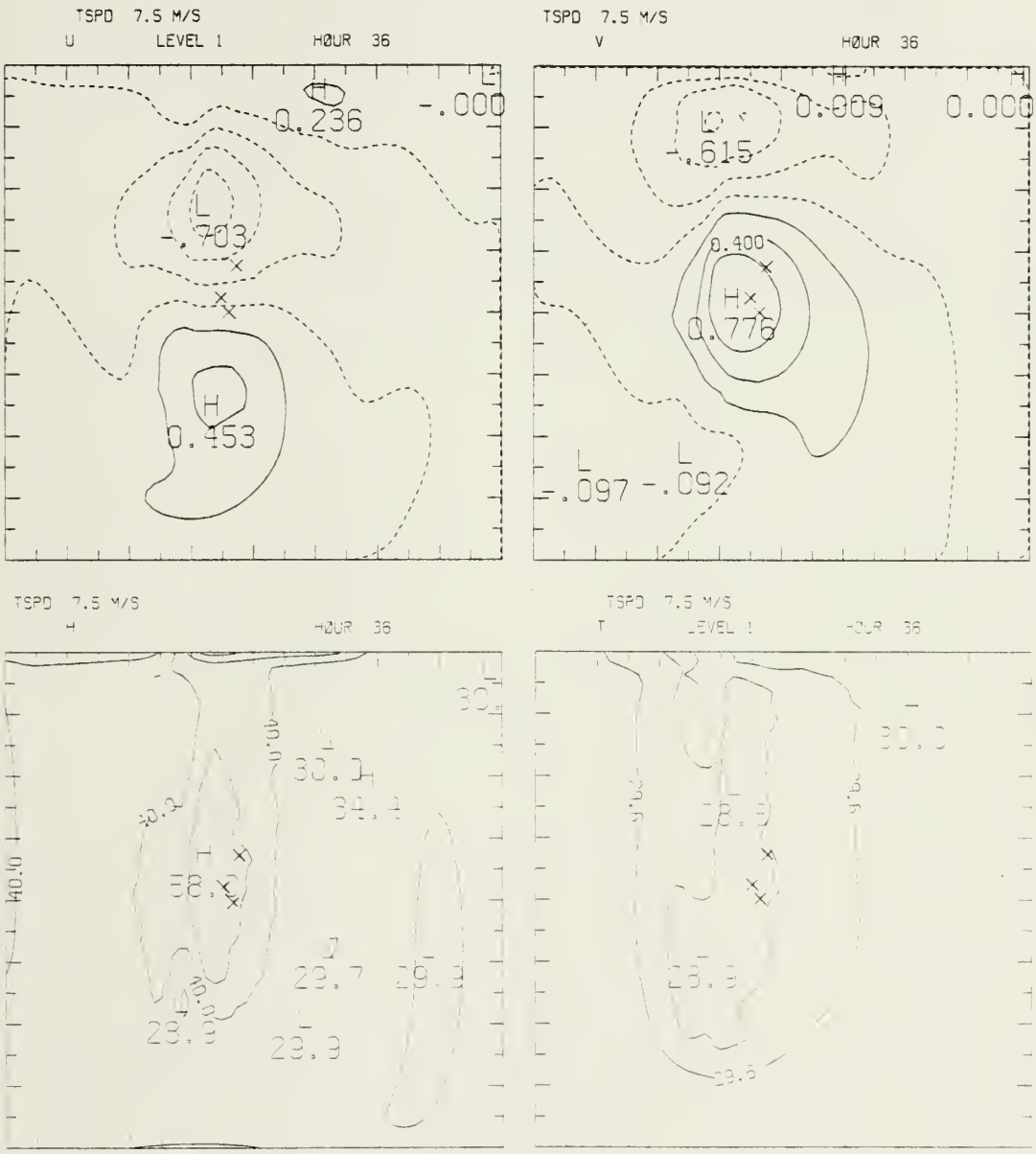

Figure 23. Model output of (a) u velocity component, (b) v velocity component, (c) mixed-layer depth, and (d) layer temperature at 36 hours.

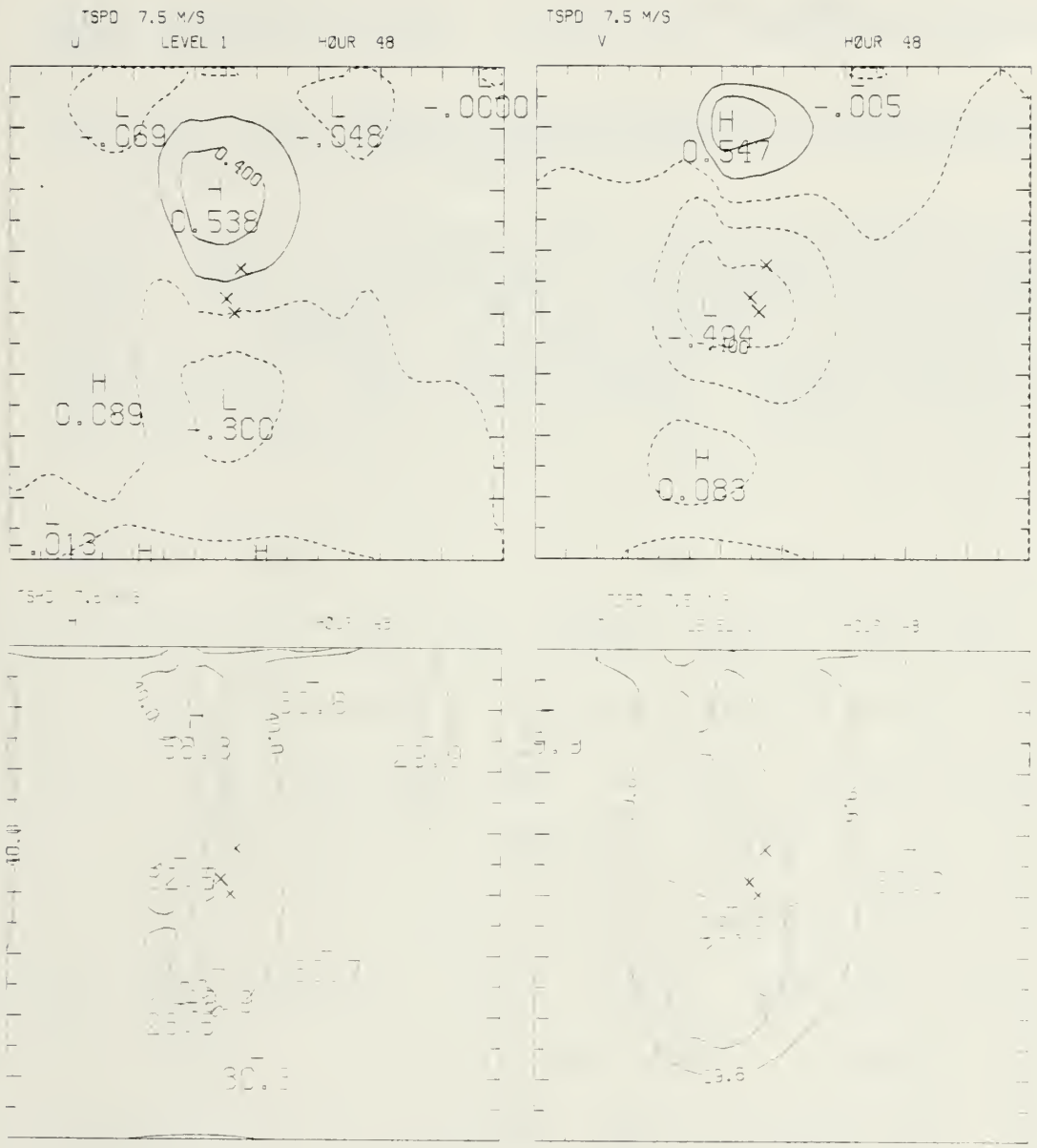

Figure 24. Model output of (a) u velocity component, (b) v velocity component, (c) mixed-layer depth, and (d) layer temperature at 48 hours.

- The resultant motion is circular over nearly the entire field with an apparent rotation period of about 24 hours.

- Current velocities in the mixed layer range from negative values of about 70 cm s^{-1} to positive values of about 80 cm s^{-1}.

- The mixed layer deepens preferentially to the right of the storm, and ranges from minimum values of about 30 m to maximum values of almost 60 m.

- A ridge of cold, upwelled water lies in the wake of the storm. This ridge is shown best in the level 3 temperature contour of Fig. 25. Superposed on this cold ridge is an upwelling/downwelling wake with an inertial period. Upwelling is in the areas of minimum MLD's (32.5 in Fig. 24c), and downwelling is in the area of maximum MLD's (58.0 in Fig. 23c). Minimum MLD's are reached at the end of the upwelling cycle and maximum MLD's are reached at the end of the downwelling cycle.

These results are consistent with the results derived from the NAVOCEANO data, which shows that the primary ocean current response to hurricane passage when no mean current exists is circular motion at the local inertial period. The reversal in flow direction every 12 hours is particularly evident in the u velocity component records for level six shown in Fig. 26. The model predictions describe the ocean response over the entire grid, rather than just at some selected points. Trajectories are plotted at several locations perpendicular to the storm track (see Fig. 27). The surface-layer trajectory that began on the left side of the track (Figs. 27a) clearly shows the surge to the left as the storm approaches, strong inertial motion following storm

passage and a net transport to the south. The trajectory along the storm path (Fig. 27b) shows a surge to the left, recovery toward the right and a small net displacement. The trajectories that began on the right (Figs. 27c and 27d) show a net deflection northward and to the right. These trajectories show that different transport profiles are expected at different locations relative to the storm. This feature is not obvious in the NAVOCEANO data due to the limited number of locations of the observations.

H. SELECTED POSITION AND DEPTH DATA

A data set similar to the NAVOCEANO data set was derived by extracting model variables at ten minute intervals at the three positions and depths shown in Table V. These time series of model variables (Figs. 28 and 29) are plotted similarly to the raw data plots of Figs. 6 and 7. The observed (Figs. 6) and predicted (Fig. 28) u-components show very similar variations although the model data are much smoother. Also, although the magnitude of the velocity component at level 2 of Fig. 28a is somewhat smaller than the 21 m magnitude shown in Fig. 6a, the magnitude at level 6 (300 m) of Fig. 28b is much smaller than the 437 m magnitude shown in Fig. 6b. The implication is that not enough

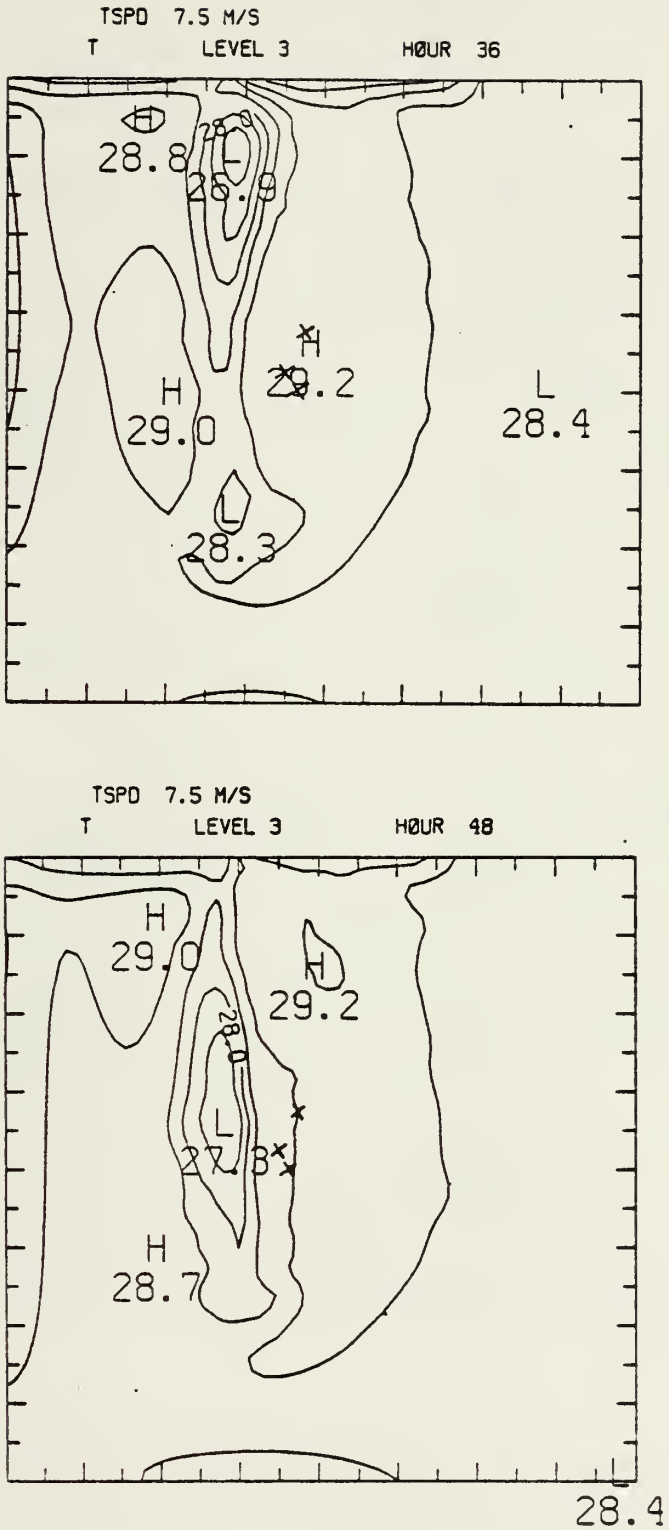

Figure 25. Model temperature prediction for level three at (a) hour 36 and (b) hour 48.

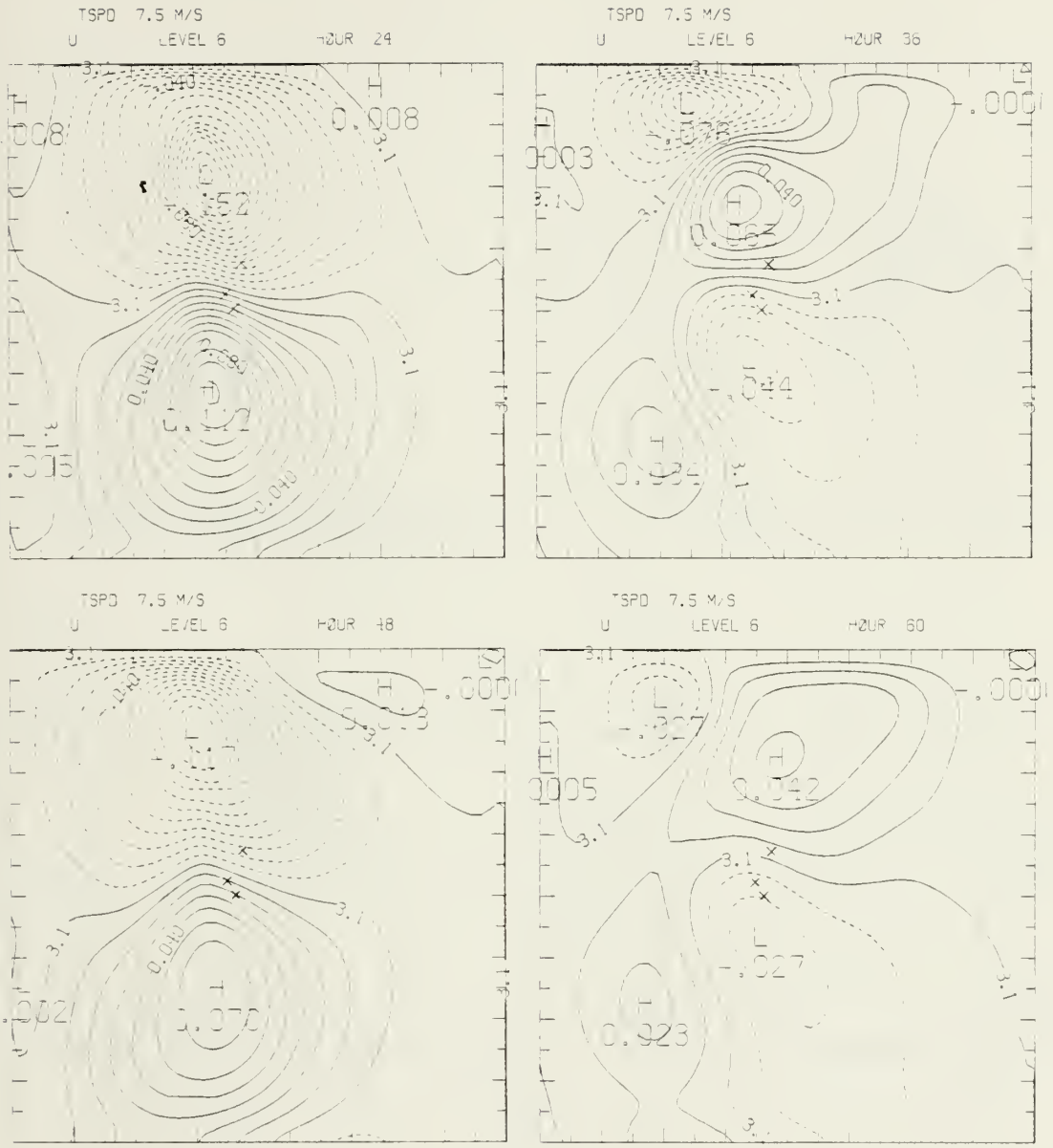

Figure 26. U velocity component at level six at (a) hour 24, (b) hour 36, (c) hour 48 and (d) hour 60 of the model run.

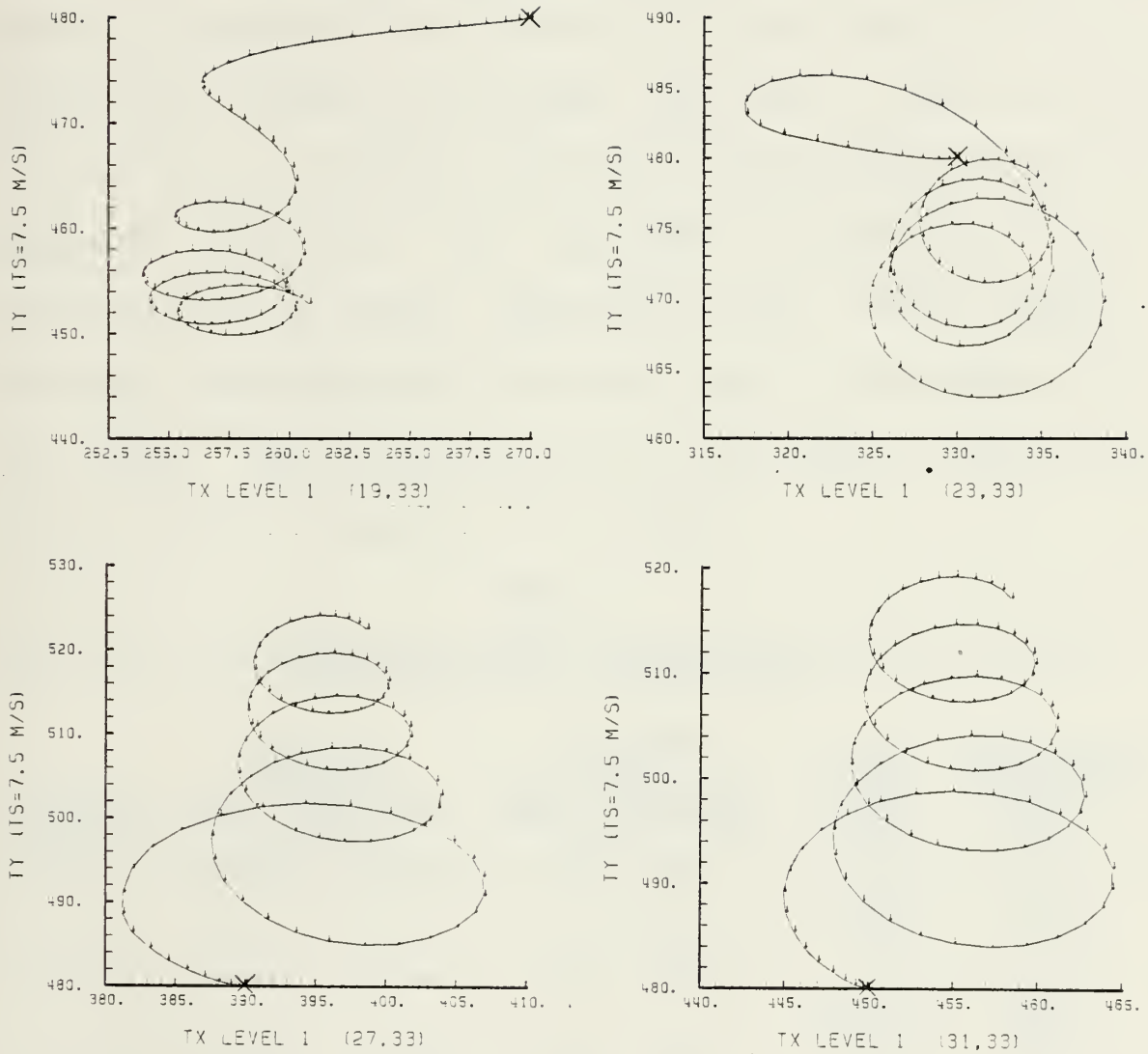

Figure 27. Trajectories for level 1 at points (a) 60 km left of, (b) along, (c) 60 km right of, (d) 120 km right of storm track. Each tick mark along the trajectory represents a 3-h displacement. X indicates the initial position of each trajectory. Notice each plot employs different spatial increments.

energy is being vertically transmitted by the model. Both the model motion and the observed flow are inertial and neither has completely damped by the end of nine days. The model u components of the velocity at levels one and six are exactly 180 degrees out of phase (Fig. 30a). That is, the velocities of the surface and bottom model layers are in the opposite directions. The NAVOCEANO velocities are also exactly out of phase immediately after storm passage, although they become more in phase later in the record (see Fig. 30b). For any given level of the model, the u and v variations are 90 degrees out of phase.

TABLE V

Positions and depths for model ten minute interval data and corresponding NAVOCEANO data.

GRID POSITION (x,y)	INERTIAL PERIOD (hours)		DISTANCE FROM STORM CENTER (km)		MID LAYER DEPTH (m)	NAVOCEANO INSTRUMENT DEPTH (m)
	MODEL	NAVOCEANO	MODEL	NAVOCEANO		
30,33	24.50	24.54	105	100	37.5	49.
					75.0	64.
					150.0	92.
29,35	24.30	24.34	90	85	19.0	19.
					150.0	179.
					300.0	324.
31,39	23.95	23.90	120	125	19.0	21.
					75.0	251.
					150.0	437.
					300.0	457.

Three-hour running averages by inertial period were computed for the extracted model data using the same technique

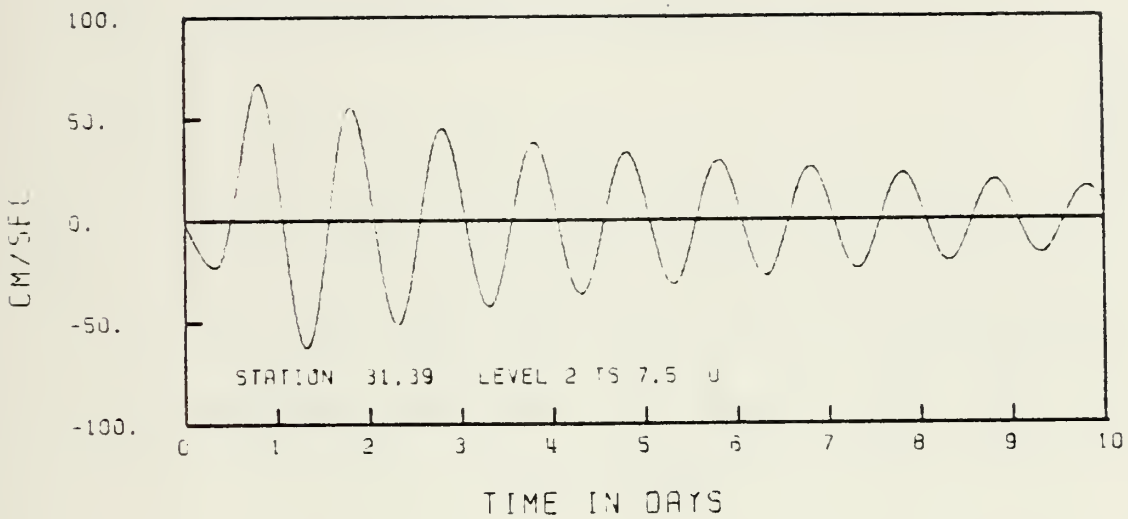

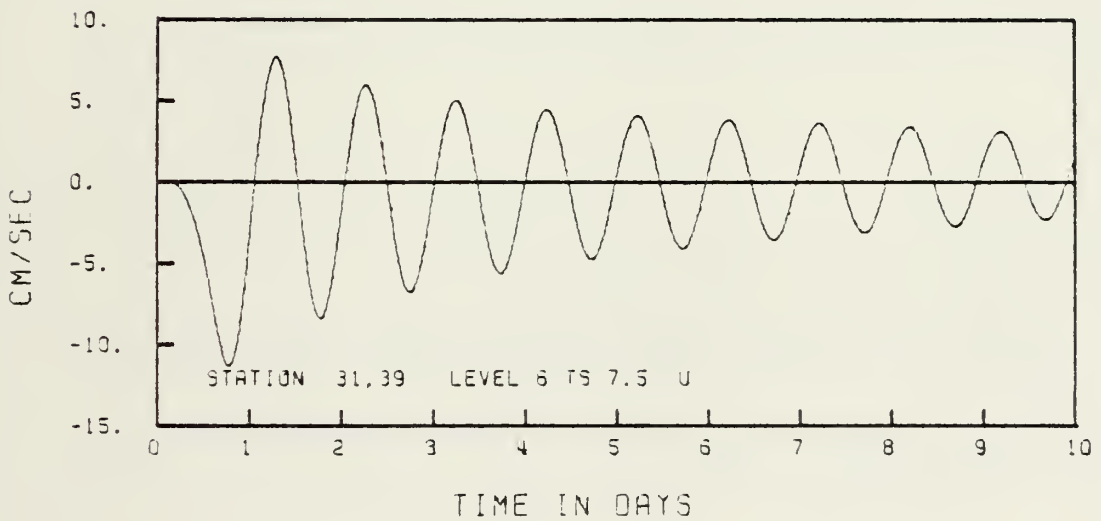

Figure 28. U components of the model current output for 10 days at mid-layer depths of (a) 19 m and (b) 300 m at station 31,39.

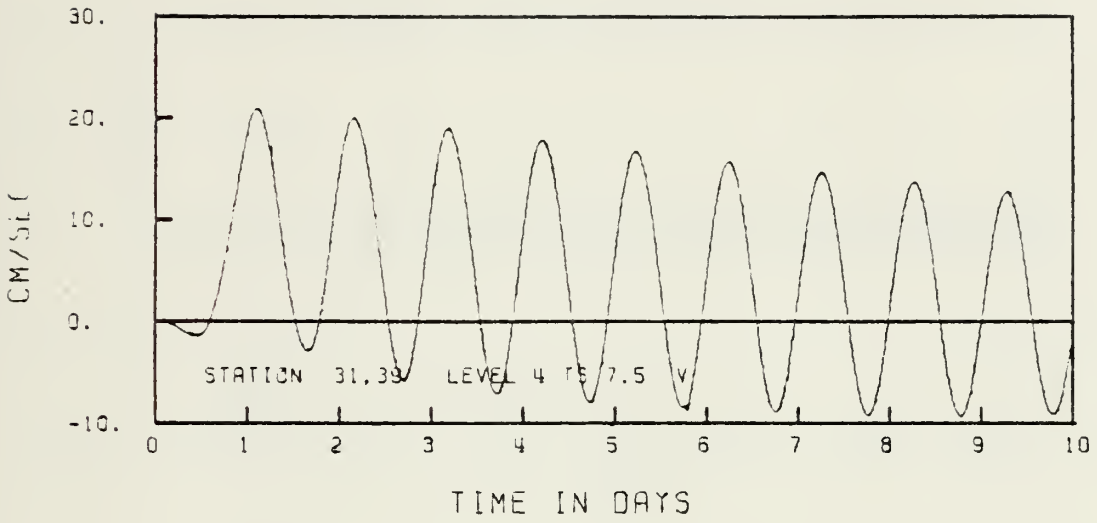

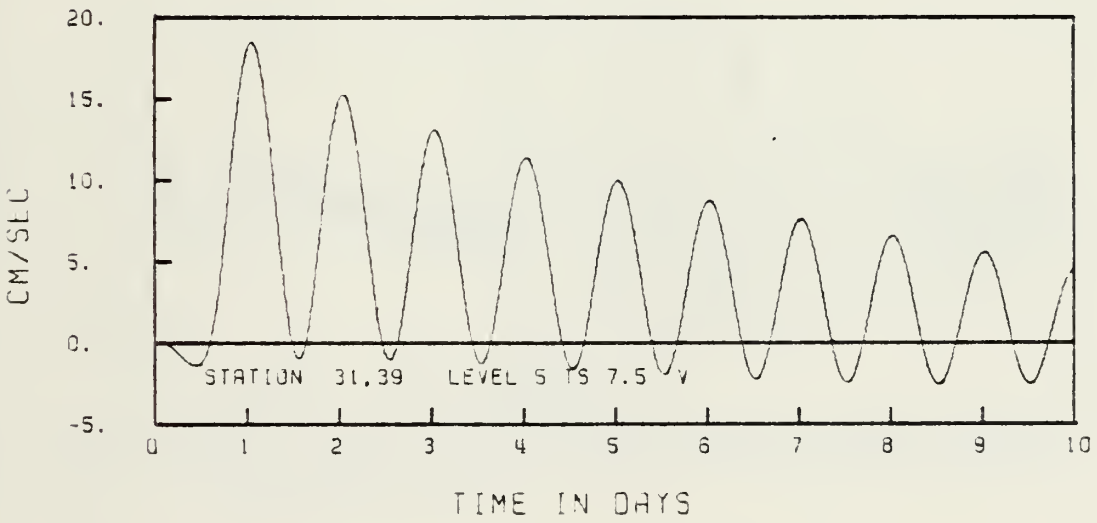

Figure 29. V components of the model current output for 10 days at mid-layer depths of (a) 75 m and (b) 150 m at station 31,39.

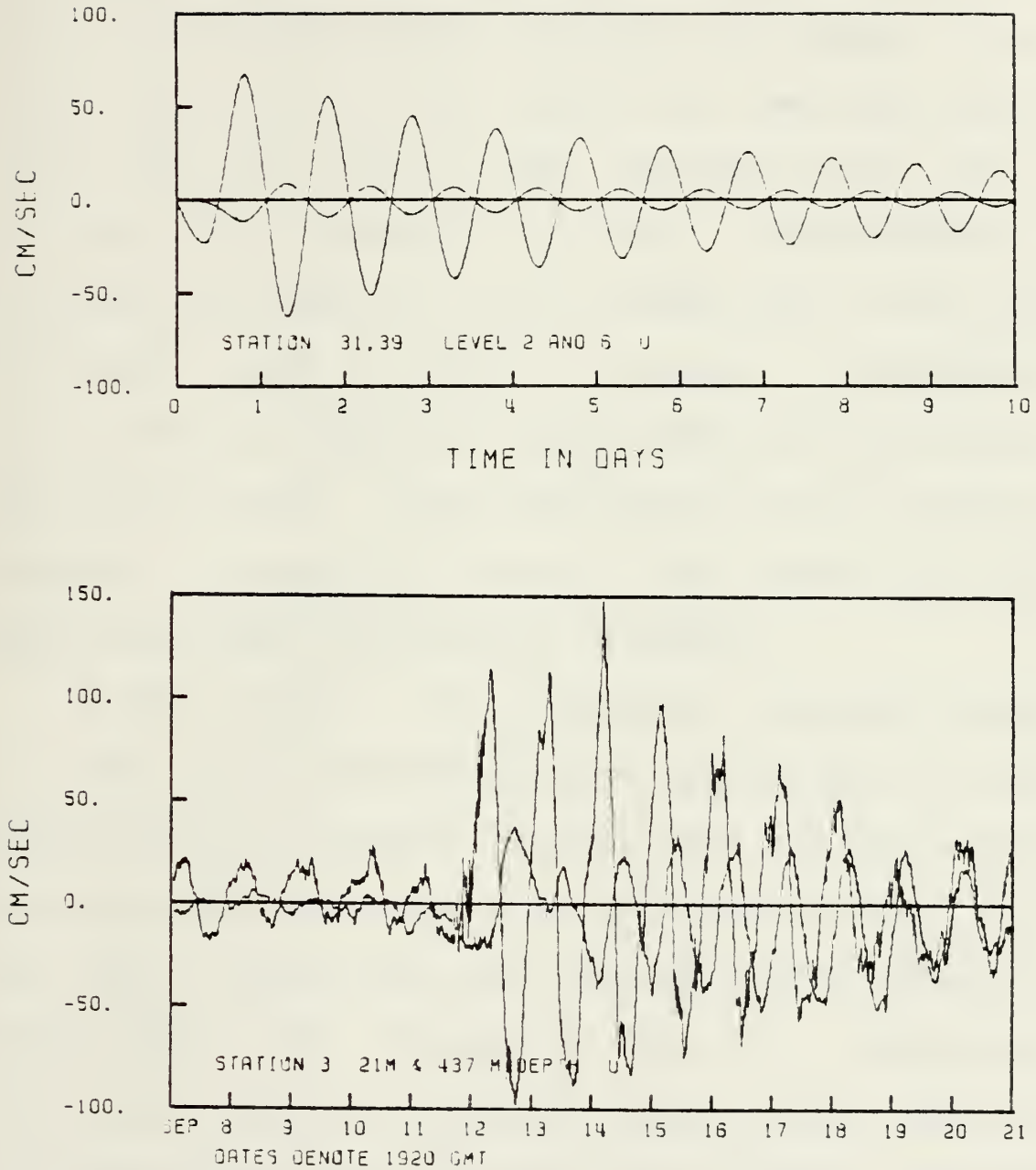

Figure 30. Superpositions of the surface and deep layer plots in (a) Fig. 23 and (b) Fig. 6.

as used for the NAVOCEANO results. A direct comparison of Figs. 13, 14 and 15 to the extracted model results running inertial period averages is made in Figs. 31, 32, 33. The model near-surface residual flows are very similar to each other (Figs. 31a and 32a), as are the lower level results (Figs. 31b, 32b and 33). Net transport to the north is indicated in all records of the model. The NAVOCEANO data indicate net transports that are closely tied to the local topography, which is absent in the model. The NAVOCEANO results also show opposite current directions for near-surface and mid depth. These observations provide interesting examples of results not shown in the model, and which require addtional investigation to explain.

In order to make a more quantitative comparison between the model and the NAVOCEANO inertial oscillations, the model results from the selected stations shown in Table V were treated in the same manner as the NAVOCEANO raw data. Circle radii, relative RMS error and mean current removed are listed (Table VII) similarly to Table II. Relative RMS errors are similar to those for station three (Table II) although maximum circle radii are not as large. Resultant calculations of energy ($cm^2\ s^{-2}$) versus inertial period are

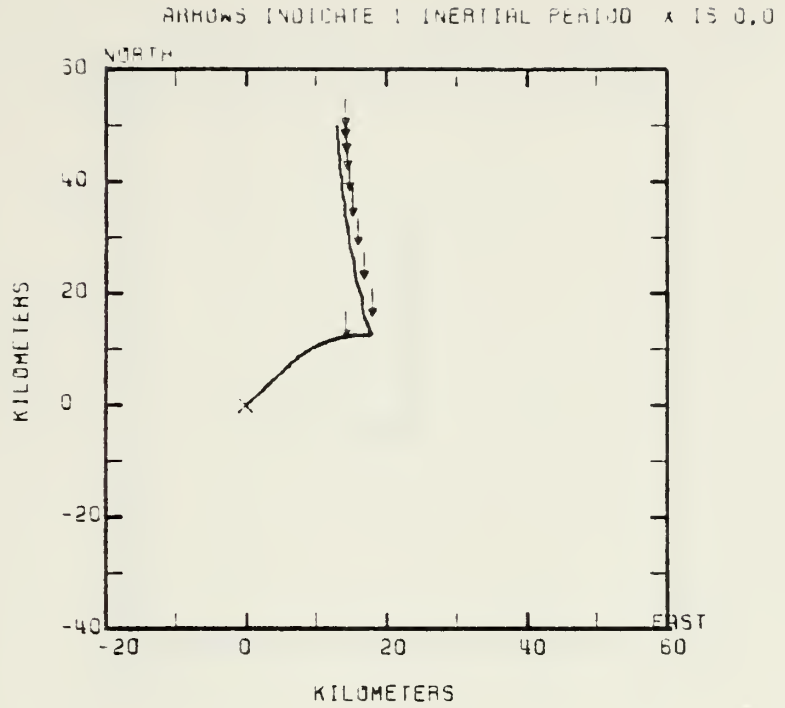

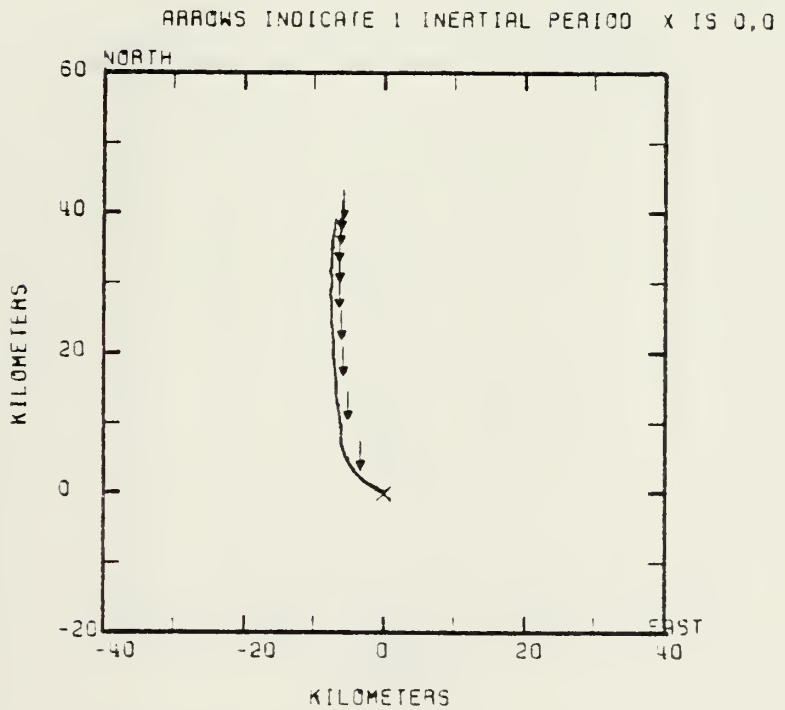

Figure 31. Running inertial period average PVD's for 10 days at (a) level 2 and (b) level 4 at grid point 31,39.

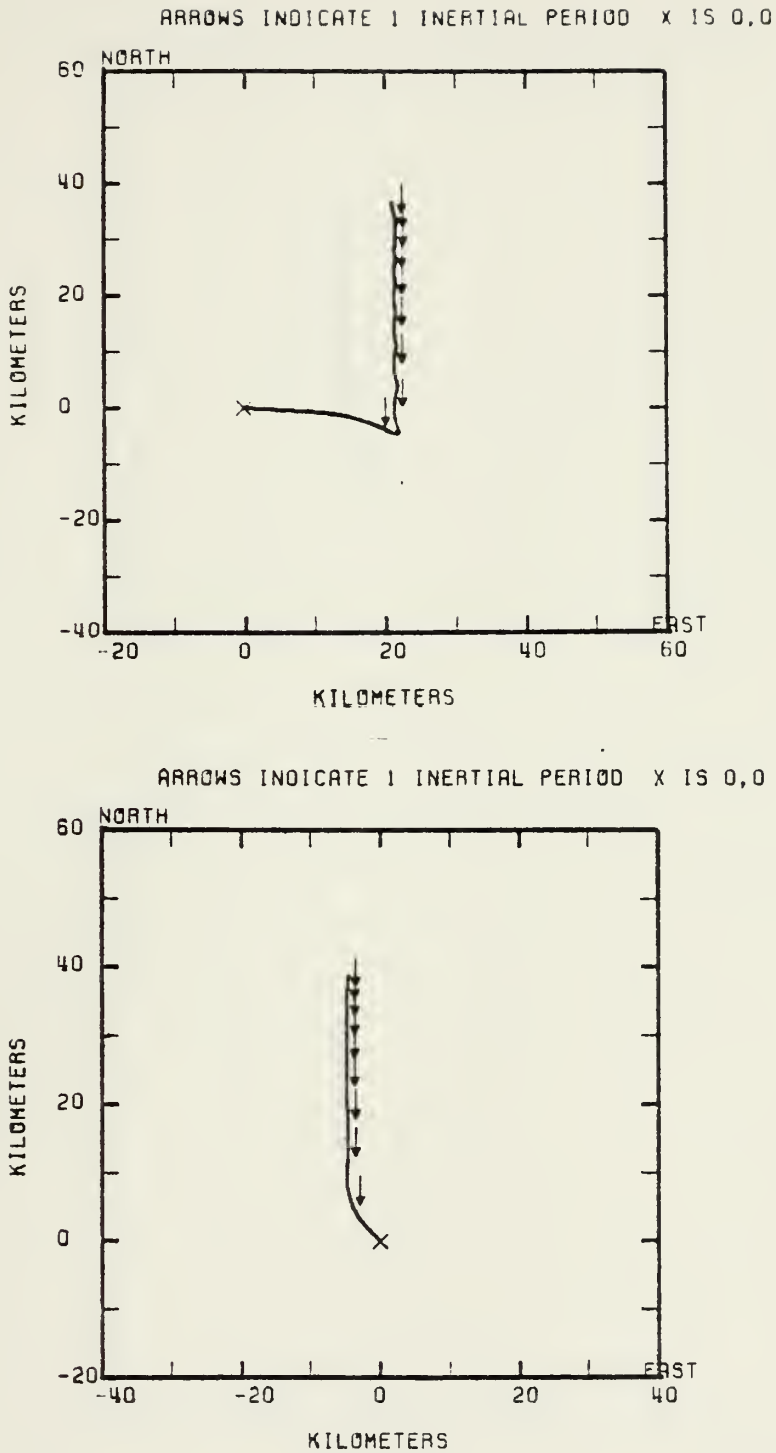

Figure 32. Running inertial period average PVD's for 10 days at (a) level 3 and (b) level 5. Level 3 is from grid point 30,33 and level 5 is from grid point 29,35.

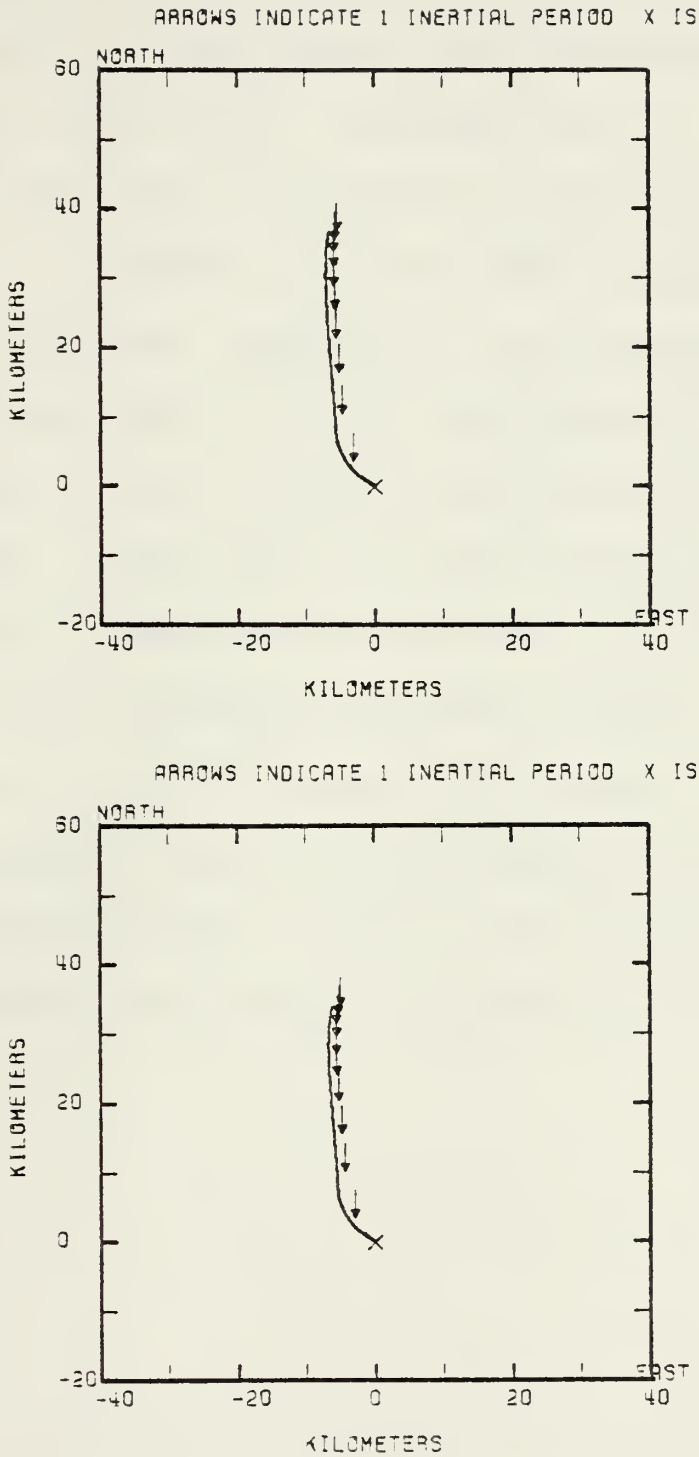

Figure 33. Running inertial period average PVD's for 10 days at (a) level 5 and (b) level 6 at grid point 31,39.

plotted (Figs. 34 and 35) similarly to the energy plots of Figs. 17 and 18. These figures show that the major differences in the model and the NAVOCEANO data, at least in a qualitative sense are in the rate of propagation of energy with depth. It appears that less energy is propagated vertically in the model compared to the observations. The energies in Figs. 35a and 35b are much smaller in comparison to the values in Fig. 34 than are the similar results of the observed data. Also, there is no slow increase in the horizontal kinetic energy near the bottom in the model as observed in the two deepest NAVOCEANO records. The level four records in Fig. 34a suggest that energy is being continually propagated into the layer because the energy levels do not appreciably decay. Detailed calculations are necessary to establish the energy flux mechanisms from the model data.

TABLE VI

Sample of circle radii, relative RMS error and mean current removed for each inertial period from the model simulation.

LEVEL ONE STATION (x, y)	INERTIAL PERIOD	RELATIVE RMS ERROR (km)	CIRCLE RADIUS (km)	CURRENT REMOVED (cm s^{-1}) u	v
(30, 33)	1	.0580	6.373	2.33	2.73
	2	.0334	10.166	-5.28	5.63
	3	.0430	6.877	-1.86	- .14
	4	.0532	5.474	-1.53	.08
	5	.0495	4.817	- .93	.25
	6	.0621	4.173	- .76	.33
	7	.0604	3.650	- .67	.35
	8	.0510	3.187	- .63	.31
	9	.0679	2.765	- .36	.37

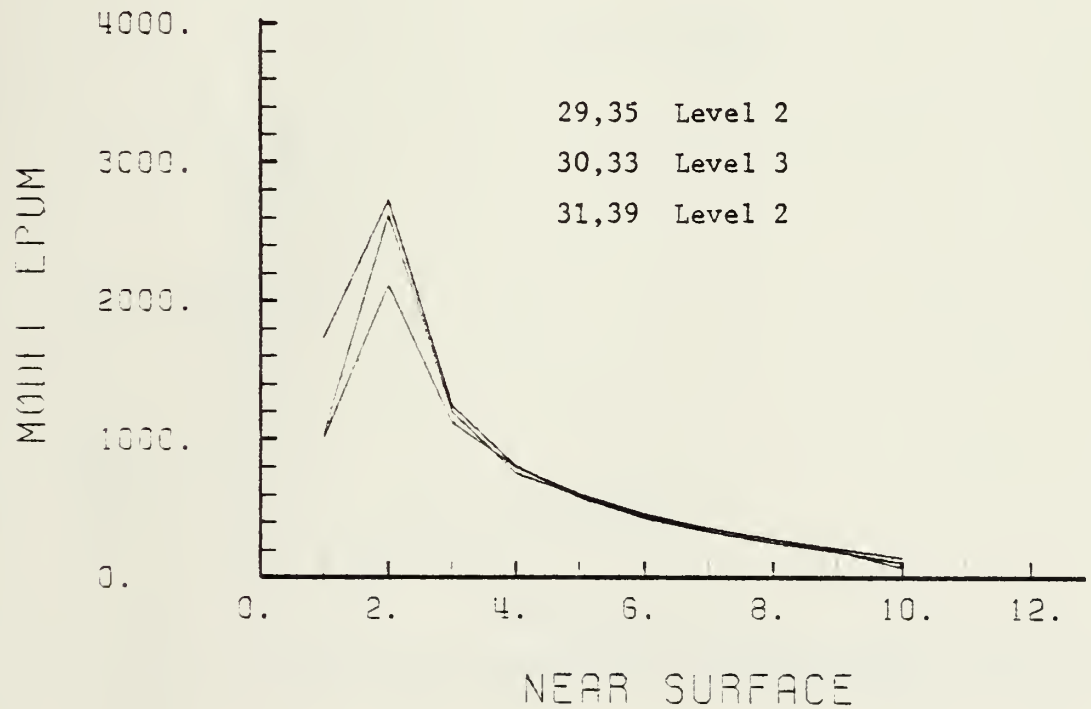

Figure 34. Energy (m^2 s^{-2}) versus inertial period at the near surface levels of grid points 30,33; 29,35 and 31,39.

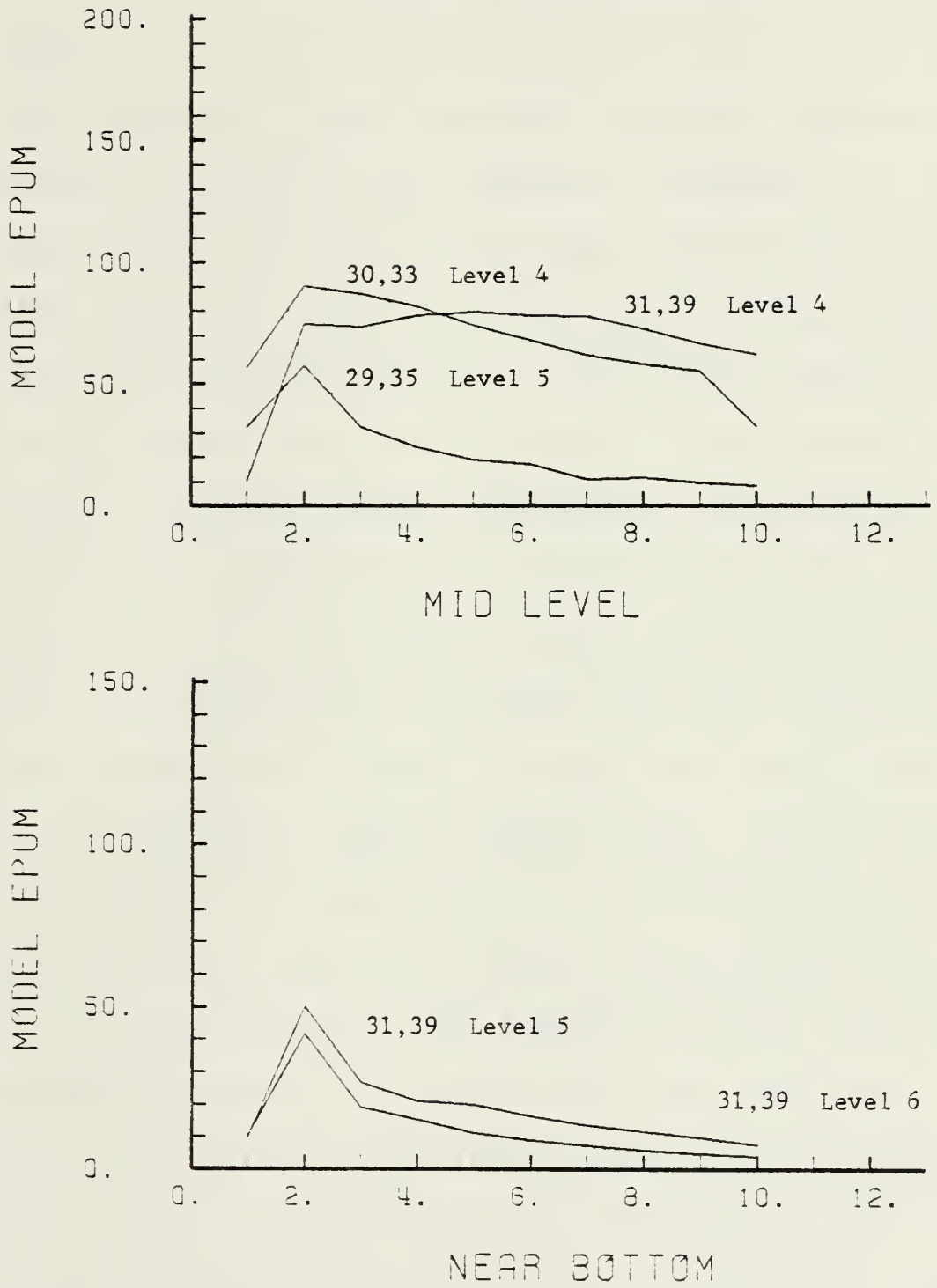

Figure 35. Energy ($m^2 s^{-2}$) versus inertial period at (a) the mid levels of each grid point in Fig. 34 and (b) the two bottom levels at grid point 31,39.

IV. SUMMARY, CONCLUSIONS AND RECOMMENDATIONS

A. SUMMARY

The NAVOCEANO data provided several physically significant results. The currents measured by the instruments were affected by topography and by the storm. The flow tended to be along the bathymetry contours except that the storm imparted a surge to the flow consistent with wind stress associated with the storm. The station one records do not depict easily identifiable inertial motion. Station one is in shallow water of about 100 meters, and shoreward motion to mid-depth is evident prior to the storm passage. An offshore flow is evident from about the time of the storm passage for a duration of about two inertial periods. The tendency at each station is for the post-storm flow to return to the same direction as the pre-storm flow. Energy input by the storm has generally dissipated by a factor of e^{-1} after three or four inertial periods, and the post-storm flow magnitude is greater than the pre-storm magnitude. The horizontal kinetic energy associated with inertial motion in the near-surface water increased more than two orders of magnitude as the storm passed and then decayed over six or seven inertial periods. At the deepest

instrument levels, the kinetic energy associated with inertial motion increased slowly and had not peaked seven inertial periods after storm passage. The mid-level instruments recorded either a sharp peak after storm passage or a less rapid increase and little decay to the end of the record depending upon location. The near-surface and near-bottom flows are about 180° out of phase for at least five or six inertial periods after storm passage.

The mixed layer-ocean circulation model results are very similar in many respects to the NAVOCEANO observations. The model does not include bathymetry, and therefore bathymetric effects are not reproduced. The model does show, however, a storm-induced surge, inertial motion damping over several inertial periods at the surface and bottom layers and different magnitudes in pre-storm and post-storm flow. The model predictions indicate an almost instantaneous near-inertial energy propagation rate with depth. The flow at the surface and at depth have the same form, increasing in magnitude and decaying at very nearly the same rate at each level. At mid levels of the model, the kinetic energy level remains nearly constant. The current oscillations in the mixed layer and in the bottom layer are 180° out of phase.

Trajectories of the model results show that the net displacement at some stations is nearly zero while at other stations the net displacement is tens of kilometers. Also, the direction of surge and of the residual flow is dependent on location relative to the storm track. The model shows a zone of upwelling/downwelling in the wake of the storm which has a near-inertial frequency.

B. CONCLUSIONS

The bathymetry of the ocean is very important in determining the direction of flow of currents at all levels. This part of the flow is not included in this ocean circulation model and must be subtracted from the real ocean data if consistent comparisons of model results and current observations are to be made. The effect of the storm is to drive the average motion in a direction consistent with the wind field of the storm. Changes in direction occur over a very short time period and are observed at all depths. As the storm passes, inertial motion results due to a balance between the centrifugal and coriolis accelerations. The kinetic energy associated with this motion remains nearly constant near the surface for two to three inertial periods and decays over an additional three to four inertial periods

to a post-storm level greater than the pre-storm level. The available data do not show the energy levels returning to the pre-storm level before the end of the record. There is an obvious time lag of the storm which increases with depth. The exact time of the initial effect at any particular depth is difficult to measure since the magnitude of the velocity does not instantaneously increase, but increases slowly with the onset of the storm. Nonetheless, the downward propagation of this energy is not instantaneous but requires on the order of one-half inertial period to propagate one-half kilometer. The energy propagates to a depth of about 450 m in one-half of an inertial period. At this depth the energy increases for at least seven to eight inertial periods. The mixed layer-ocean circulation model closely simulates the inertial motion and damping rates near the surface. The vertical propagation of energy is not, however, very similar to the NAVOCEANO observations. The model does provide insight into the three-dimensional ocean and is impressive in distinguishing between results at locations varying with respect to the storm center.

C. RECOMMENDATIONS

The primary differences between the NAVOCEANO data and the model results are in the vertical propagation of kinetic energy associated with storm passage. Further research is required to isolate the mechanism of energy propagation so that it can be included in the model formulation.

LIST OF REFERENCES

Adamec, D., R.L. Elsberry, R.W. Garwood, Jr. and R. L. Haney, 1981: An embedded mixed-layer--ocean circulation model, Dynamics of Atmospheres and Oceans, 6, 69-96.

Black, P.G., and G. Withee, 1976: The effect of Hurricane Eloise on the Gulf of Mexico (abstract). Bull. Amer. Meteor. Soc., 57, 139.

Fedorov, K.N., A.A. Varfolomeev, A.I. Ginzburg, A.G. Zatsepin, A. Yu. Krasnopevtsev, A.G. Ostrovsky, and V.E. Skylarov, 1979: Thermal reaction of the ocean on the passage of the hurricane Ella, Oceanology, 19, 992-1001 (in Russian).

Fisher, E.L., 1958: Hurricanes and the sea surface temperature field, J. Meteorology, 15, 328-333.

Friese, L.V., 1977: Response of the upper ocean to Hurricane Eloise, M.S. Thesis, Naval Postgraduate School, Monterey, California, 53 pp.

Garwood, R.W., Jr., 1977: An oceanic mixed-layer model capable of simulating cyclic states, J. Phys. Oceanogr., 7, 455-468.

Geisler, J.E., 1970: Linear theory of the response of a two layer ocean to a moving hurricane, Geophys. Fluid Dyn., 1, 249-272.

Haney, R.L., 1980: A numerical case study of the development of large-scale thermal anomalies in the central north Pacific Ocean, J. Phys. Oceanogr., 10, 541-556.

Huh, O.K., W.J. Wiseman, Jr., and L.J. Rouse, Jr., 1981: Intrusion of Loop current Waters onto the west Florida continental shelf, J. Geophys. Res., 86, 4186-4192.

Hurlburt, H.E., and J.D. Thompson, 1980: A numerical study of Loop Current intrusions and eddy shedding, J. Phys. Oceanogr., 10, 1611-1651.

Leipper, D.F., 1967: Observed ocean conditions and Hurricane Hilda, J. Atmos. Sci., 24, 182-196.

Leipper, D.F., 1970: A sequence of Current Patterns in the Gulf of Mexico, J. Geophys. Res., 75, 637-687.

Mayer, D.A., H.O. Mofjeld, and K.D. Leaman, 1981: Near-inertial waves observed on the outer shelf in the middle Atlantic bight in the wake of Hurricane Belle, J. Phys. Oceanogr., 11, 87-106.

Martin, P.J., 1982: Mixed-layer simulation of buoy observations taken during hurricane Eloise, J. Geophys. Res., 87, 409-427.

Molinari, R.L., 1978: An overview of the circulations in the Gulf of Mexico, Summary Report: Working Conference on the Circulations in the Gulf of Mexico, W. Sturges and S.L. Shang, Ed., Dept. of Oceanography, Florida State University, 29-30.

Price, J.F., 1981: Upper ocean response to a hurricane, J. Phys. Oceanogr., 11, 153-175.

Pudov, V.D., A.A. Varfolomeev, and K.N. Fedorov, 1979: Vertical structure of the wake of a typhoon in the upper ocean, Okeanologiya, 21, 142-145.

U.S. Navy, 1965: Oceanographic atlas of the north atlantic ocean, section I: tides and currents, U.S. Navy Oceanographic Office, Washington, D.C., 73 pp.

Withee, G.W., and A. Johnson, 1976: Data report: buoy observations during hurricane Eloise (September 19 to October 11, 1975), U.S. Dept. of Commerce, National Oceanic and Atmospheric Administration, NSTL Station, Mississippi, 21 pp.

Wright, R., 1969: Temperature structure across the Kuroshio before and after typhoon Shirley, Tellus, 21, 409-413.

INITIAL DISTRIBUTION LIST

		No. Copies
1.	Defense Technical Information Center Cameron Station Alexandria, VA 22314	2
2.	Library, Code 0142 Naval Postgraduate School Monterey, CA 93940	2
3.	Professor Robert J. Renard, Code 63Rd Department of Meteorology Naval Postgraduate School Monterey, CA 93940	1
4.	Professor Christopher N. K. Mooers, Code 68Mr Department of Oceanography Naval Postgraduate School Monterey, CA 93940	1
5.	Professor Russell L. Elsberry, Code 63Es Department of Meteorology Naval Postgraduate School Monterey, CA 93940	5
6.	Professor R. William Garwood Jr., Code 68G Department of Oceanography Naval Postgraduate School Monterey, CA 93940	1
7.	Lt. Charles K. Hopkins PCO New Jersey (BB 62) Long Beach Naval Shipyard Long Beach, CA 90807	1
8.	Director Naval Oceanography Division Naval Observatory 34th and Massachusetts Avenue NW Washington, D.C. 20390	1
9.	Commander Naval Oceanography Command NSTL Station Bay ST. Louis, MS 39522	1
10.	Commanding Officer Naval Oceanographic Office NSTL Station Bay St. Louis, MS 39522	1
11.	Commanding Officer Fleet Numerical Oceanography Center Monterey, CA 93940	1

12. Commanding Officer 1
Naval Ocean Research and Development Activity
NSTL Station
Bay ST. Louis, MS 39522

13. Commanding Officer 1
Naval Environmental Prediction Research Facility
Monterey, CA 93940

14. Chairman, Oceanography Department 1
U.S. Naval Academy
Annapolis, MD 21402

15. Chief of Naval Research 1
800 N. Quincy Street
Arlington, VA 22217

16. Office of Naval Research (Code 480) 1
Naval Ocean Research andDevelopment Activity
NSTL Station
Bay ST. Louis, MS 39522

17. Scientific Liaison Office 1
Office of Naval Research
Scripps Institution of Oceanography
La Jolla, CA 92037

18. Library 1
Scrippps Institution of Oceanography
P.O. Box 2367
La Jolla, CA 92037

19. Library 1
Department of Oceanography
University of Washington
Seattle, WA 98105

20. David Adamec, Code 63Ac 1
Department of Meteorology
Naval Postgraduate School
Monterey, CA 93940

21. Commander 1
Oceanographic Systems Pacific
Box 1390
Pear Harbor, HI 96860

22. Chief, Ocean Services Division 1
National Oceanic and Atmospheric Administration
8060 Thirteenth Street
Silver Springs, MD 20910